Reading Nature's Book by Looking, More than Once, at its Cover

An Axiom-Free Relativity Theory Based on Direct Physical Measurements

(First unedited draft – December 12, 2015)

Ramzi Suleiman

University of Haifa

Al Quds University

Please address all correspondence to Dr. Ramzi Suleiman, University of Haifa, Haifa 31509, Israel.

Email: suleiman@psy.haifa.ac.il, Mobile: 972-(0)50-5474- 215.

Reading Nature's Book by Looking, More than Once, at its Cover

An Axiom-Free Relativity Theory Based on Direct Physical Measurements

Table of Contents

Reading Nature's Book by Looking, More than Once, at its Cover

An Axiom-Free Relativity Theory Based on Direct Physical Measurements

Abstract

We consider inertial physical systems in which signals about physical measurements conducted in one reference-frame are transmitted to a receiver moving with relative constant velocity v, by an information carrier with a constant velocity v_c with respect to transmitter's rest-frame. To render the model relevant to reality we assume that $v_c > v$. We make no other assumptions. For systems of this type we derive the relativistic time, distance, mass, and energy transformations, relating measurements transmitted by the information sender to the corresponding information registered at the receiver. The sender and receiver need not be human or animate observers. The resulting relativistic terms are simple and beautiful. They are functions only of the normalized velocity $\beta = \dfrac{v}{v_c}$, implying that they are *scale independent* with respect to the velocity of the information carrier, and mass and spatial dimensions of the observed bodies. The model's scale independency renders it applicable for all physical systems, irrespective of their size, and velocity of the information carrier used in the system. For $\beta \ll 1$, all the derived transformations reduce to Galileo-Newton physics.

The derived transformations disobey the Lorentz invariance principle. The time transformation predicts relativistic time *dilation* for distancing bodies and time *contraction* for approaching bodies. The distance transformation predicts relativistic length *contraction* for approaching bodies and length *extension* for distancing bodies. The mass transformation is conjugate to the distance transformation, implying increase in relativistic mass density for approaching bodies and decrease of mass density for distancing bodies, due to respective length contraction or extension along the body's travel path. For distancing bodies the relativistic kinetic energy as function of β displays a monotonic pattern with a unique maximum at one maximum at $\beta = \Phi$, where Φ is the golden ratio ($\approx$ 0.618). At sufficiently high normalized velocities, the relativistic extension can maintain spatial

locality between distanced particles, suggesting that quantum entanglement is not "spooky" since it is a proximal action.

For the special case of $v_c = c$, where c is the velocity of light, application of the proposed model to yields new important insights and results and reproduces several important predictions of Special Relativity, General Relativity, observationally based ΛCDM models, and Quantum Theory. The model makes excellent predictions of for the Michelson-Morley's "null" result, the relativistic lifetime of decaying Muons, the Sagnac effect, and the neutrino velocities reported by OPERA and other collaborations. Application of the model to cosmology, without alteration or addition of free parameters, is successful in accounting for several cosmological findings, including the pattern of recession velocity predicted by inflationary theories, the amounts of matter and dark energy in various segments of redshift, reported in recent ΛCDM cosmologies, the GZK energy suppression phenomenon, and the radius of gravitational black holes. . 3 In reference [3] we show that Epistemic Relativity, despite being a deterministic and local ("non-spooky"), accounts, both qualitatively and quantitatively, for entanglement in a bipartite preparation like the one described in the famous EPR paper. In reference [4] we extended the analysis in [3] and showed that the theory is successful in explaining, both qualitatively and quantitatively, the matter-wave duality, quantum criticality and phase transition. More strikingly, the model account successfully for several quantum phenomena, including quantum criticality, entanglement and formation of Bose-Einstein condensates. Comparison between the dynamics of dark energy and quantum energy leaves no doubt that dark energy is the cosmic twin of quantum energy, exhibiting the same dynamics on cosmic scales.

The multiplicity and range of the proposed epistemic model predictions, suggests that for inertial systems, mere observation of moving bodies is a potent tool for extracting the laws of nature as they are revealed to us. Put metaphorically we contend that the hidden secrets of the book of Nature often disclose themselves, by leaving fingerprints on the book's cover. From observing the fingerprints, humans and other beings can reconstruct information valuable for their survival.

"Nature is pleased with simplicity. And Nature is no dummy".

Sir Isaac Newton

1. Introduction and Theory

In this paper we take a completely new approach to the study of inertial systems involving the dynamics of moving bodies. Our approach is epistemic and deterministic. We deal only with observable or measurable physical variables. We analyze the simple, yet very general case of a physical system in which two observers move with constant linear velocity (v) with respect to each other, while communicating information about physical observables, such as time durations of events, lengths of objects and their masses and kinetic energies. We assume that information about observations and measurements taken by one observer in his or her rest-frame are communicated to the second observer by an information carrier with a constant velocity v_c with respect to information transmitter's rest-frame. For rendering the situation practical we assume that $v_c > v$. We make no additional assumptions. We compare the information measured in one frame, by the corresponding information received in the second frame. The sender and receiver may not be human observers. For two reference frames moving with constant velocity v with respect to each other, Table 1 depicts the resulting information transformations about time duration, distance, mass and kinetic energy (for

complete derivations, see supporting information). In the table, the variables Δt_0, Δx_0, and ρ_0 denote measurements of time duration, distance, and the body's mass density in the rest frame, respectively, $\beta = \frac{v}{v_c}$, and $e_0 = \frac{1}{2} \rho_0 \, v_c{}^2$.

Table 1

Epistemic Relativity Theory's Transformations

Physical Term	Relativistic Expression	
Time	$\dfrac{\Delta t}{\Delta t_0} = \dfrac{1}{1-\beta}$	.... (1)
Distance	$\dfrac{\Delta x}{\Delta x_0} = \dfrac{1+\beta}{1-\beta}$	.... (2)
Mass	$\dfrac{\rho}{\rho_0} = \dfrac{1-\beta}{1+\beta}$	.... (3)
Kinetic energy	$\dfrac{e_k}{e_0} = \dfrac{1-\beta}{1+\beta} \beta^2$	... (4)

As eq. (1) shows, Epistemic Relativity disobeys the Lorentz Invariance principle. It predicts time dilation with respect to distancing bodies, and time *contraction* with respect to approaching bodies. Note that eq. (1) resembles the Doppler formula for wave travel [1-2], which predicts red-shift or blue-shift, depending on whether the wave-source is distancing from or approaching the observer. The relativistic distance term (eq. 2) prescribes length contraction for approaching bodies and length *extension* for distancing bodies. The mass transformation is conjugate to the distance transformation, implying an increase in relativistic mass density for approaching bodies and decrease of mass density for distancing bodies, due to respective length contraction, or extension, along the body's travel path. For approaching bodies the relativistic kinetic energy density increases monotonically and quite sharply with the normalized relative velocity β, while for distancing bodies it displays a non-monotonic dependence on velocity, with a unique maximum at one maximum at $\beta = \Phi$, where Φ is

7

the golden ratio (≈ 0.618). As shown in fig 1. As figure 1 shows the relativistic kinetic energy increases monotonically, reaching a maximum at a transitional velocity equaling $\beta_t = \Phi$, where Φ is the famous Golden Ration ($\frac{\sqrt{5}-1}{2} \approx 0.618$) [4-5], after which it declines more rapidly, reaching zero for $\beta = 1$. No less interesting, the maximal value of the relativistic kinetic energy at the transition point is equal to Φ^5 or ≈ 0.09016994.
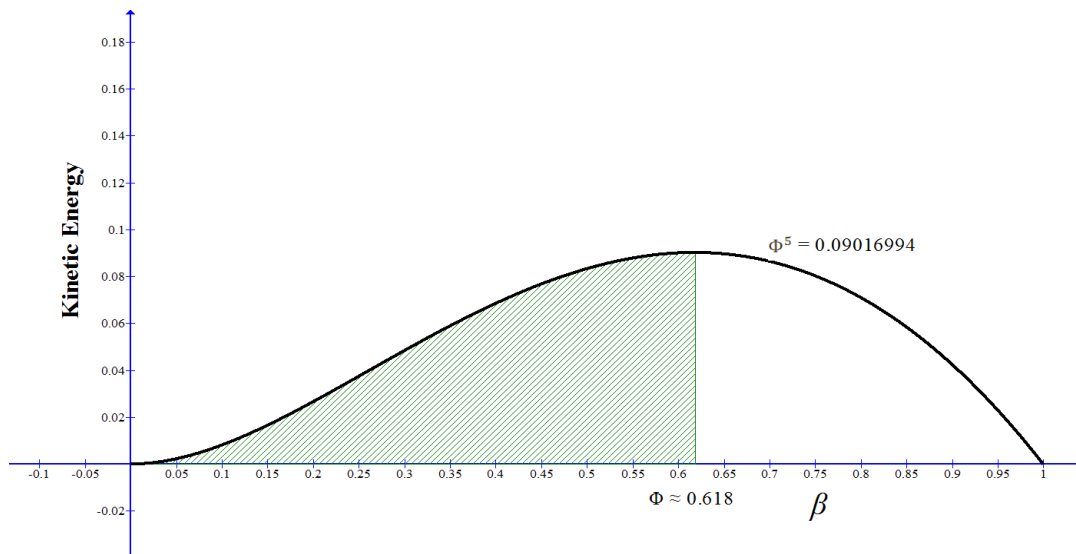
Figure 1. Kinetic energy as a function of velocity

The transformations in the table have some nice properties: First, they are deterministic and simple. Second, for low velocities $\beta \ll 1$, all the transformations reduce to the classical Newtonian formulas. Third, the theory satisfies the EPR necessary condition for theory *completeness*, in the sense that every element of the physical reality has a counterpart in the physical theory [3]. Fourth, the theory is *scale independent with respect to the size of the investigated physical system*. It applies to the dynamics of very small and very large bodies, suggesting the dynamics of the too small and too large bodies abide by the same laws of physics. Fifth, the theory is also *scale independent with respect to the information carrier's velocity v_c*, (provided that $v_c > v$), suggesting it could also be

8

applied to the dynamics of moving bodies in classical physical systems (e.g., acoustic, thermal, seismic, etc.).

The non-axiomatic nature of the proposed epistemic model and its simplicity and beauty are undoubtedly three desirable, provided that the model can make good predictions of real phenomena. In the following sections we provide convincing evidence for the success of the our epistemic approach in predicting many experimental and observational results in elementary particles physics, quantum mechanics, and cosmology. To save space, the derivations of some of the results are given in the Supporting Information.

2. Application to Elementary particles dynamics

We demonstrate here that Epistemic Relativity performs as well as Special Relativity predicting important findings concerning the dynamics of elementary particles, including the famous Michelson-Morley experiment [6] , the Frisch and Smith time dilation in muon decay experiments [7] and the relativistic time gains reported in "around-the-world atomic clocks" experiment [8]. We also demonstrate that Epistemic Relativity yields excellent predictions for two types of experiments, which could not be accounted for by Special relativity: The Sagnac effect [9-10] and the neutrino velocity reported in recent experiments conducted by OPERA and other collaborations [11-16].

2.1 Michelson-Morley's null result

Background:

In their seminal paper [6], Michelson and Morley (M&M) reported an experiment set to test the velocity of the motion of Earth in the presumed. M&M analyzed the motion of the parallel and perpendicular waves (with respect to Earth's motion). They found (incorrectly) that the displacement of the interference fringes is given by: $2\ D_0(\frac{v}{c})^2\ =\ 2\ D_0\beta^2$, where D_0 is the interferometer arm's length at rest. It is well known that the results of the M&M experiment, and many subsequent experiments [e.g., 48-53], were far less than the above prediction. As M&M reported, "Considering the motion of the earth in its orbit only, this displacement should be $2\ D_0(\frac{v}{c})^2\ =\ 2\ D_0$ x 10^{-8}. The

distance D was about 11 meters, or 2×10^7 wavelengths of yellow light; hence, the displacement to be expected was 0.4 fringes. The actual displacement was certainly less than the 20th part of this (prediction) and probably less than the 40th part," ([6], p. 341) which is "too small to be detected when masked by experimental errors" ([6], p. 337).

It is well-known that *SR* was successful in predicting the M&M null result without Inclusion of the notion of ether, and that by this, it opened a new era of post-Newtonian physics. Here, we show that the Epistemic Relativity performs as well as *SR* in predicting the null effect.

Prediction

To account for the relativistic effects on the distance that light travels in the round trip, we replace $2D_0$ by $D_1 + D_2$ in the equation derived by M&M, where D_1 and D_2 are the departure and arrival distances, respectively. Using the distance transformation depicted in Table 1, we get:

$$\text{Fringe Shift} = (D_1 + D_2)\, \beta^2 = D_0 \left(\frac{1+\beta}{1-\beta} + \frac{1-\beta}{1+\beta} \right) = D_0 \frac{1+\beta^2}{1-\beta^2} \beta^2 \qquad \dots (5)$$

Where $\beta = \frac{v}{c}$, $c \approx 299792.458\ km/_s$, and v is the velocity of Earth around the ($v \approx 29.78\ km/_s$).

Substituting $\beta = \frac{29.78\ km/_s}{299792.458\ km/_s} \approx 9.9340 \times 10^{-5}$ and $D_0 = 11$m (the interferometer's arm length in the M&M experiment) in eq. (5), we obtain a predicted fringe shift of approximately 1.09 x 10^{-7}, which is five orders of magnitude smaller than the reported experimental resolution (of ≤ 0.02). The comparable prediction made by SR is $2\,D\,\beta^2 = 2\,D_0\,(\sqrt{1-\beta^2}\,\beta^2)$, which after substitution yields $\approx$ 1.97x 10^{-8}. Given the resolution in the M&M experiment, the difference between the two predictions ($\approx$ 8.9 x 10^{-8}) is negligible. Table 2 summarizes similar calculations performed for several M&M type experiments, while contrasting them with the respective predictions of SR.

Table 2

Predictions of findings reported by classical Michelson-Morley type experiments

Experiment	Arm length (meters)	Expected Fringe shift	Measured Fringe shift	Resolution	ER prediction	SR prediction
Michelson and Morley [6]	11.0	0.4	< 0.02 or ≤ 0.01	0,01	$\approx 4.34 \times 10^{-7}$	$\approx 4.34 \times 10^{-7}$
Miller [17]	32.0	1.12	≤ 0.03	0.03	$\approx 1.27 \times 10^{-6}$	$\approx 1.26 \times 10^{-6}$
Tomaschek [18]	8.6	0.3	≤ 0.02	0.02	$\approx 3.40 \times 10^{-7}$	$\approx 3.40 \times 10^{-7}$
Illingworth [19]	2.0	0.07	≤ 0.0004	0.0004	$\approx 7.89 \times 10^{-8}$	$\approx 7.90 \times 10^{-8}$
Piccard & Stahel [20]	2.8	0.13	≤ 0.0003	0.0007	$\approx 1.11 \times 10^{-7}$	$\approx 1.11 \times 10^{-7}$
Michelson et al. [21]	25.9	0.9	≤ 0.01	0.01	$\approx 1.02 \times 10^{-6}$	$\approx 1.02 \times 10^{-6}$
Joos [22]	21.0	0.75	≤ 0.002	0.002	$\approx 8.30 \times 10^{-7}$	$\approx 8.30 \times 10^{-7}$

As the table shows, both theories predict the null results. Moreover, the differences between the predictions of Epistemic Relativity and Special Relativity are either zero or in the order of magnitude of 10^{-10}.

2.2. Time dilation of decaying muons

Background

In muon-decay experiments, muons are generated when cosmic rays strike the upper levels of the Earth's atmosphere. They are unstable, with a life time of $\tau = 2.2\ \mu s$. With counters that count muons traveling within a velocity of 0.99450**c** to 0.9954**c**, comparing their flux density at both the top and bottom of a mountain gives the rate of their decay. In the most famous muon-decay experiment [7], assuming a velocity of 0.992c of muons in air, researchers found that the percentage of the surviving muons descending from the top of Mt. Washington to the sea level (d ≈ 1907 m.) was (72.2 ± 2.1) %, considerably higher than 36.79%, the expected percentage resulting from non-relativistic calculation.

Prediction

To calculate the relativistic muon decay, denote the times at Earth and at a moun's frame by t and t', respectively. Without loss of generality, assume that at the mountain's level, $t = t' = 0$. For any time t' $(0 \le t' \le t'_B)$, where t'_B is the muon's time arrival at the bottom, the flux density $N(t')$ could be expressed as:

$$N(t') = N(0)\ e^{-\frac{t'}{\tau}}, \qquad\qquad\qquad \text{..... (6)}$$

where $N(0)$ is the count at the mountain's level. Substituting the value of t' from eq. (4), we get:

$$N(t)_{CR} = N(0)\ e^{-\frac{(1-\beta)t}{\tau}}. \qquad\qquad\qquad \text{..... (7)}$$

A similar analysis based on SR yields

$$N(t)_{SR} = N(0)\ e^{-\frac{\sqrt{1-\beta^2}\ t}{\tau}}. \qquad\qquad\qquad \text{..... (8)}$$

For $\beta = 0.992$, Figure 3 depicts the rates of decay predicted by Epistemic Relativity, Special Relativity, and a nonrelativistic calculation. For an ascending time of $\delta t = \frac{d}{v} = \frac{1907\ m.}{2.998 \times 10^8} \approx 6.36$ μs., the predictions of Epistemic Relativity and Special Relativity are, respectively, $\frac{N(t=6.36)_{CR}}{N(0)}$ x 100=

$e^{-\frac{(1-0.992)x\,6.36}{2.2}}$ x $100 \approx 97.7\%$ and $\frac{N(t=6.36)_{SR}}{N(0)}$ x $100 = e^{-\frac{\sqrt{1-0.992^2}\,x\,6.36}{2.2}}$ x $100 \approx 69.42\%$. By contrast,

according to nonrelativistic considerations, the expected percentage of surviving muons is only

$\frac{N(t=6.36)_{NR}}{N(0)}$ x $100 = e^{-\frac{6.36}{2.2}}$ x $100 \approx 5.55\%$. Comparison with the observed percentage of 72.2%

strongly indicates that a classical analysis fails to account for the observed phenomenon, whereas the

two relativistic approaches succeed in achieving that. Note that the predicted values of both theories

are not precise, given the fact that the theoretical calculations ignore several factors affecting the

flight of descending particles [23].
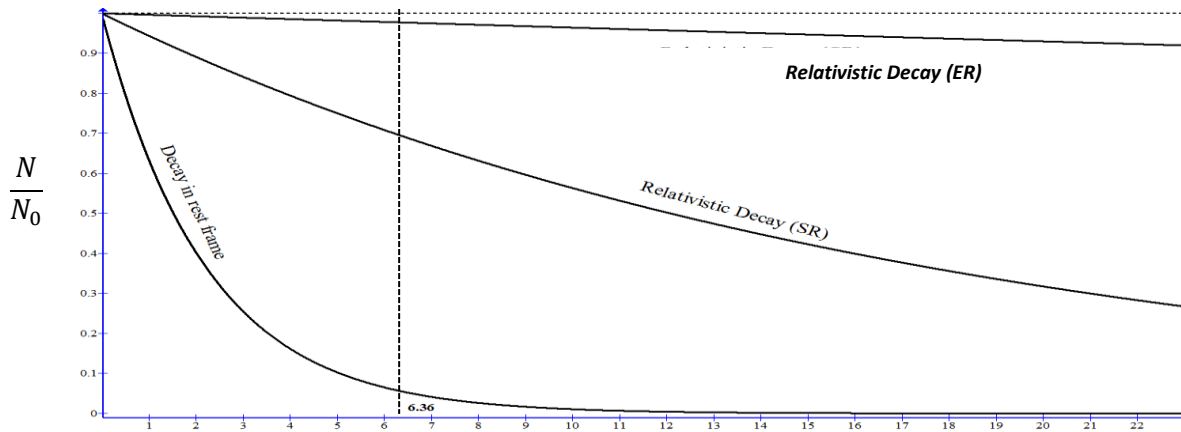
Figure 2: Predicted rates of muon decay

2.3 Around the World Atomic Clocks experiments

Around the world type of experiments represent a direct way to test the time dilation prediction

using highly accurate atomic carried by aircrafts flying eastward or westward around the world (see

e.g., [8]). Given the relatively low velocity of airliners compared with the velocity of light, such

experiments, in similarity to the M&M experiments are incapable of discriminating between *Special*

Relativity and Epistemic Relativity, since, as will be shown hereafter, both theories yield almost

identical predictions.

For an "around the world trip", Special Relativity's time dilation is given by:

$$\tau_{SR} = \frac{t}{t'} = \frac{2}{\sqrt{1-\beta^2}}, \quad \beta = \frac{v}{c} \qquad \qquad \ldots .. (10)$$

While Epistemic Relativity's prediction is:

$$\tau_{IR} = \frac{t}{t'} = \left(\frac{1}{1-\beta} + \frac{1}{1+\beta}\right) = \frac{2}{1-\beta^2} \qquad \qquad \ldots .. (11)$$

Figure 4 depicts the predictions of Special Relativity and Epistemic Relativity for relatively low velocities.
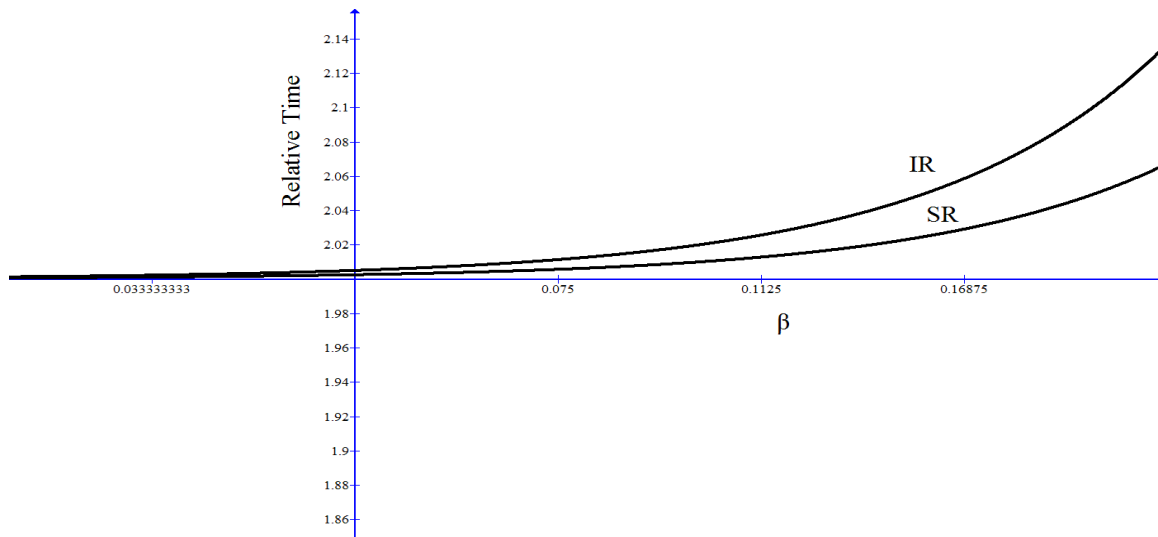
Figure 3: predictions of Special Relativity and Epistemic Relativity for relatively low velocities

For a cruising air speed for long-distance commercial passenger flights, the estimated velocity is 475–500 knots (878-926 km/h). The resulting difference in relative time between Special Relativity and Epistemic Relativity predictions for this speed range is ≈0.0007, which requires for its detection a measurement sensitivity of at least 4 degrees of magnitude more than the sensitivity of measurements reported in [8].

2.4 Sagnac effect

Background

The Sagnac effect, named after its discoverer in 1913 [24], has been replicated in many experiments (for reviews, see [25-29]). The Sagnac effect has well-known and crucial applications in navigation [29] and in fiber-optic gyroscopes (FOGs) [30-34]. In the Sagnac effect, two light beams, sent clockwise and counterclockwise around a closed path on a rotating disk, take different time intervals to travel the path. For a circular path of radius R, the time difference can be represented as $\Delta t = \frac{2\,v\,l}{c^2}$, where $v=\omega\,R$ and l is the circumference of the circle ($l=2\pi R$). Today, FOGs have become highly sensitive detectors measuring rotational motion in navigation. In the GPS system, the speed of light relative to a rotating frame is corrected by $\pm\,\omega\,R$, where ω is the radial velocity of the rotating frame and R is the rotation radius. A plus/minus signs is used depending on whether the rotating frame is approaching the light source or departing from it, respectively.

Many physicists claim that because the Sagnac effect involved a radial motion, it does not contradict SR and that it should be treated in the framework of general relativity [35-36]. However, Wang at al. [9, 10] strongly refute this claim in two well-designed experiments that show unambiguously that an identical Sagnac effect appearing in uniform radial motion occurs in linear inertial motion. For example, Wang et al. [9] tested the travel-time difference between two counter-propagating light beams in uniformly moving fiber. Contrary to the LI principle and to the prediction of SR, their findings revealed a travel-time difference of $\frac{2v\,\Delta l}{c^2}$, where Δl is the length of the fiber segment moving with the source and detector at a v, whether the segment was moving uniformly or circularly. This finding in itself should have raised serious questions about the validity of the LI principle and SR. If the Sagnac effect can be produced in linear uniform motion, then the claim that it is a characteristic of radial motion is simply incorrect. Because the rules SR apply to linear uniform

motion, the only conclusion is that SR is incorrect. Strikingly, the unrefuted detection of a linear Sagnac effect and its diametrical contradiction with SR has hardly been debated.

Prediction

Applying Epistemic Relativity to the linear Sagnac experiment yields the following difference between the arrival times of the two light beams:

$$\Delta t = \frac{\Delta l}{c-v} - \frac{\Delta l}{c+v} = \frac{2v\,\Delta l}{(c-v)(c+v)} = \frac{2v\,\Delta l}{c^2 - v^2} \approx \frac{2v\,\Delta l}{c^2} \ , \qquad\qquad\qquad \dots (12)$$

Which is in agreement with the analysis and results reported in [9].

2.5 Neutrino velocity

Background

In 2011, the OPERA collaboration at CERN announced that neutrinos had travelled faster than light [37]. The reported anticipation time was 60.7 ±6.9 (stat.)± 7.4 (sys.) ns, and the relative neutrino velocity was $\frac{v-c}{c}$ = (5.1 ±2.9) $\times 10^{-5}$. The excitement that swept physicists and laymen concerning the possibility that a new era was "knocking on physics doors" waned a few months later, after OPERA reported the discovery of hardware malfunctions in the GPS system, which resulted in a critical measurement error.   After accounting for the error, the anticipation time was only $(2.7 \pm 3.1$ (stat.) $+ {}^{+3.8}_{-2.8}$ (sys.)) $\times 10^{-6}$, with corresponding $\frac{v-c}{c}$ = 2.67 x 10 $^{-6}$ [11]. Since then, the OPERA and several collaborations, including ICARUS, LVD, and Borexino, have replicated the "null" result [12-15]. The only "faster-than-light" result of which we are aware of was reported in 2007 by the MINOS collaboration [16], who reported an early anticipation time of 126 ± 32 (stat.) ± 64 (sys.) ns

(C.L. = 68%), with corresponding $\frac{v-c}{c}$ = 5.1±2.9 (stat.+sys.)×10^{-5}. However, the high statistical and system errors reported by MINOS impede the validity of the above quoted result.

Prediction

For a typical neutrino-velocity experiment, consider a neutrino that travels a distance *d* from a source (e.g., at CERN) and arrives at a detector (e.g., at Gran Sasso). According to Epistemic Relativity, such an experiment includes *three* frames: the neutrino frame *F*, the source frame *F′*, and the detector frame *F″*. *F* is departing from *F′* with velocity *v* and approaching *F″* with velocity – *v*. *F′* and *F″* are at rest relative to each other. Derivation of the term $\frac{v-c}{c}$ for a typical neutrino velocity experiments (see section II in SI) yields:

$$\frac{v-c}{c} = \sqrt[2]{\frac{2}{1-\frac{c\,\delta t}{d}} - 1} - 1 \qquad \dots (13)$$

Where *d* is the travel distance. δt is the *early* neutrino arrival time with respect to the velocity of light c. For the OPERA-corrected result [29], *d* = 730.085 km and δt = (6.5 ± 7.4 (stat.) ± $^{+9.2}_{-6.8}$ ($sys.$)) ns. Substituting in eq. (13), we get:

$$\frac{v-c}{c} = \left(\frac{2}{1-\frac{299792.458\,x\,6.5\,x\,10^{-9}}{730.085}} - 1\right)^{\frac{1}{2}} - 1 \approx - 2.67 \text{ x } 10^{-6} \qquad \dots (14)$$

Which is almost identical to the reported result of $\frac{v-c}{c}$ ($Exp.$) = (2.7 ± 3.1 ($stat.$) ± $^{+3.8}_{-2.8}$ (sys.)) ×10^{-6}. Applying eq. (13) to five other experiments, conducted by MINOS, OPERA, ICARUS, LVD, and Borixeno collaborations, yields the results summarized in Table 3.

Table 3

Predictions of ER for six neutrino-velocity experiments

Experiment	Experimental $\frac{v-c}{c}$	Predicted $\frac{v-c}{c}$
OPERA 2012 (corrected result) [11]	$(2.7 \pm 3.1\,(\text{stat}.) + ^{+3.8}_{-2.8}\,(\text{sys.})) \times 10^{-6}$	2.67×10^{-6}
OPERA 2013 [12]	$(-0.7 \pm 0.5\,(\text{stat}.) + ^{+2.5}_{-1.5}\,(\text{sys.})) \times 10^{-6}$	-0.66×10^{-6}
ICARUS 2012 [13]	$(0.4 \pm 2.8(\text{stat.}) \pm 9.8\,(\text{sys.})) \times 10^{-7}$	0.41×10^{-7}
LVD [14]	$(1.2 \pm 2.5(\text{stat.}) \pm 13.2\,(\text{sys.})) \times 10^{-7}$	1.23×10^{-7}
Borexino [15]	$(3.3 \pm 2.9(\text{stat.}) \pm 11.9\,(\text{sys.})) \times 10^{-7}$	3.28×10^{-7}
MINOS 2007 [16]	$(5.1 \pm 2.9)\,)(\text{stat}) \times 10^{-5}$	5.14×10^{-5}

As the table shows, the mode yields precise predictions for all the tested experiments.

3. Application to Quantum Mechanics

3.1 Background

Quantum phenomena are empirically proven properties of nature with tremendous potential for future technologies. In particular, quantum entanglement has applications in emerging technologies of quantum computing and quantum cryptography, and quantum teleportation experimentally. A short list of exciting developments includes Ekert's pioneering invention of a secure cryptographic key [38-39], quantum communication dense coding [40-41], and teleportation experiments, starting

from pioneering experiments (e.g., [42-43]), to more recent experiments on teleportation in different scenarios (see, e.g., [44-45]).

For many decades, quantum theory has been gaining much success in predicting quantum entanglement and other quantum phenomena. The common view of current physics adopts the assertion of Bell's theorem that no theory of nature that obeys locality and realism can reproduce the predictions of quantum theory [46-48]. Einstein, Podolsky, and Rosen formalized the most serious object to the nonlocality of quantum theory in their famous EPR paper [3]. In essence, the paper argues the *nonlocality* prescribed by quantum theory implies the theory is incomplete, such that its elements are not in one-to-one correspondence with physical reality. EPR concluded by asserting that the wave function does not provide a complete description of the physical reality. , EPR concluded their seminal paper by posing the rhetoric question of whether a complete description of physical reality exists, and reply to it by stating: "We believe, however, that such a theory is possible" (see in [3], p. 780).

John Bell formalized the EPR deterministic world idea in terms of a local *hidden variable*s model (LHVM). The LHVM assumes (1) measurement results are determined by properties the particles carry prior to, and independent of, the measurement ("realism"), (2) results obtained at one location are independent of any actions performed at space-like separation ("locality"), and (3) the setting of local apparatus are independent of the hidden variables that determine the local results ("free will") [49]. Bell proved the above assumptions impose constraints on statistical correlations in experiments involving bipartite systems, in the form of the famous Bell inequality. He then showed that the probabilities for the outcomes obtained when suitably measuring some entangled quantum states violate Bell's inequality. He concluded that entanglement is that feature of quantum formalism that makes simulating the quantum correlations within any classical formalism impossible. It is now commonly accepted by physicists that the correlations predicted by quantum mechanics and observed in experiments reject the principle of local realism and with it the possibility of "hidden

variables" as a mediator of information about one system state to a distanced system. However, the restriction put by Bell's inequality on local and realistic theories is based on the presumption that non-locality between two distanced particles is synonymous to "faster-than-light" causation [46]. Bell was very concerned with this temporal aspect *of non-locality*, perhaps due the contradiction it created between quantum mechanics and Special relativity theory. In Bell's words, "We have an apparent incompatibility, at the deepest level, between the two fundamental pillars of contemporary theory" (Bell, 1984, p. 172, quoted in [49]). However, John Bell did not pay attention, whatsoever, to the possibility of special locality between distanced particles. As a result Bell's Theorem gives no regard to this dimension of locality, nor did the numerous experimental tests of the theory (e.g., [50-55]. Researchers might have never entertained the possibility of spatial locality between distanced particles, because our intuition and common sense tell that particles that are distanced from each other become spatially disconnected. This intuition, however, has never been tested experimentally.

It follows that Bell's inequality cannot forbid the proposed model of being a candidate for reproducing the results of quantum mechanics. With this "pass" at hand, we proceed by demonstrating that Epistemic Relativity is in fact successful in reproducing the predictions of quantum theory for key phenomena, including matter-wave duality, quantum phase transition, quantum entanglement and the formation of Bose-Einstein condensate.

3.2 Matter-Wave Duality

The concept of matter-wave duality is central to quantum theory, ever since 1924, when Louis de Broglie introduced the notion [58-59]. Nonetheless, it remains a strange and unexplained phenomenon. Here we show that Epistemic Relativity sheds a new light on this issue by demonstrating that it is a natural consequence of relativity. To show this we use a setup involving a simple closed system in inertial linear motion. Specifically, we consider a particle of rest mass m_0 which travels along the positive x axis, with constant velocity v away from the rest frame F of

another particle. Denote the "traveling" particle's rest frame by F'. The kinetic energy of the particle, as function of the relative velocity $\beta = v/v_c$ (see eq. 8), is depicted by the continuous line in Fig.1. The dotted line in the figure corresponds to the classical Newtonian term. At very low velocities relative to the information carrier velocity, the bulk of the particle's energy is carried by its matter while at high enough velocities, relative to the carrier velocity, the particle's energy is carried by the particle's wave (see fig. 4). Thus, although completely different in its approach, Epistemic Relativity's description of the matter-wave is akin to de Broglie's matter-wave model. Interestingly, Epistemic Relativity predicts that the relativistic body's matter and wave energies are equal at normalized velocity $\beta = \dfrac{1}{3}$.

The difference, shown by the dashed line, corresponds to the energy carried by the body's wave. Formally we define the body's wave energy at a given velocity as the difference between the matter's Newtonian energy term e_0 and its relativistic energy term e_k, or:

$$e_w \ = \ e_0 \ - \ e_k \ = \frac{1}{2} \rho_0 \, v_c{}^2 \, \beta^2 \ \ -\frac{1}{2} \rho_0 \, v_c{}^2 \, \frac{1-\beta}{1+\beta} \beta^2 \ \ = \left(\frac{1}{2} \rho_0 \, v_c{}^2\right) \frac{2\beta^3}{1+\beta} = \frac{2\,\beta^3}{1+\beta} \, e_0 \ .. \ (19)$$

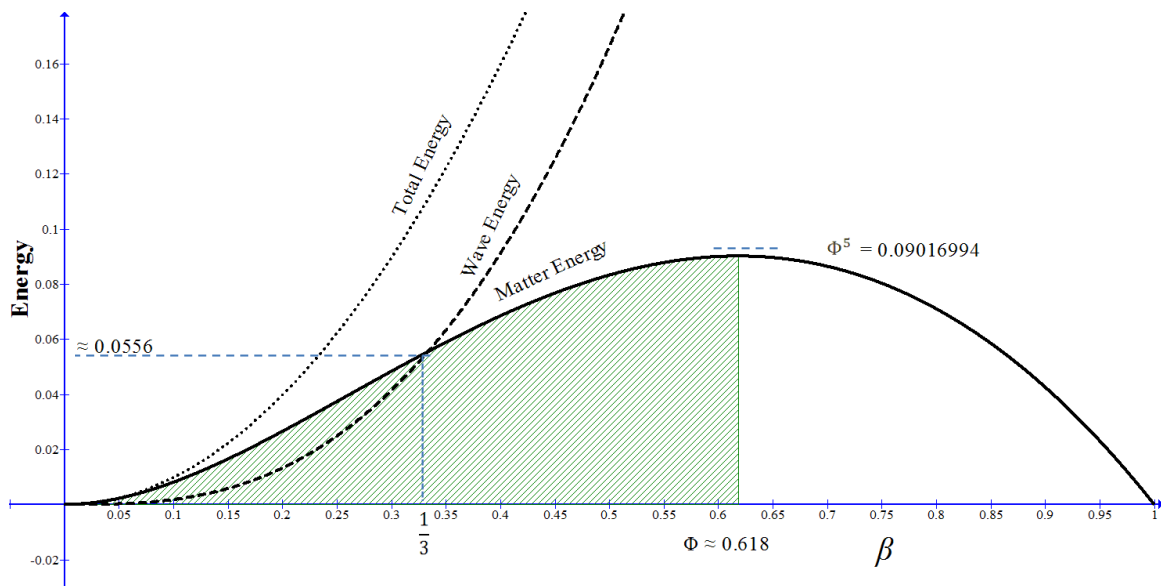Where $e_0 = \dfrac{1}{2} \rho_0 \, v_c{}^2.$

Figure 4. Matter energy and wave energy as functions of velocity

21

3.3 Matter Phase Transition

Figure 4 reveals that the predicted particle's wave energy increases quite sharply with β. In contrast; the matter energy function is non-monotonic with β. It increases up to a maximum and then decreases to zero at $\beta = 1$.

The critical velocity β_{cr} at which the matter energy achieves its maximum value can be obtained by deriving e_k in eq. 8 with respect to β and equating the derivative to zero, which yields (see section c in SI):

$$\beta^2 + \beta - 1 = 0 \qquad \dots (20)$$

Which for $\beta \neq 0$ solves for:

$$\beta_{cr} = \frac{\sqrt{5}-1}{2} = \Phi \approx 0.618 \qquad \dots (21)$$

Where Φ is the famous Golden Ratio [4] . Substituting β_{cr} in the eq. 19 yields:

$$\frac{(e_k)_{max}}{e_0} = \Phi^2 \frac{1-\Phi}{1+\Phi} \qquad \dots (22)$$

From eq. 20 we can write: $\Phi^2 + \Phi - 1 = 0$, which implies $1 - \Phi = \Phi^2$ and $1 + \Phi = \frac{1}{\Phi}$.

Substitution in eq. 22 gives:

$$\frac{(e_k)_{max}}{e_0} = \Phi^5 \approx 0.09016994 \qquad \dots (23)$$

The above result is precisely equal to Hardy's maximum probability of obtaining an event which contradicts local realism [60]. More importantly, the point of maximum marks a point of matter phase transition, at which matter becomes critically quantum. Up to this point ($0 < \beta < \Phi$) the relationship between energy and velocity is semi-classical, in the sense that higher velocities are associated with higher matter energies, while for ($\Phi < \beta < 1$), higher velocities are associated with lower matter energies. This result confirms with a recent experimental result by Coldea *et al*. [61] who

demonstrated that applying a magnetic field at right angles to an aligned chain of cobalt niobate atoms, makes the cobalt enter a quantum critical state, in which the ratio between the frequencies of the first two notes of the resonance equals the Golden Ratio.

The critical point of matter phase transition could be described in terms of the relativistic extension, or "stretch" $\hat{l}$, defined as l/l_0. From eq. 6 we can write:

$$\beta = \frac{\hat{l}-1}{\hat{l}+1} \qquad \dots (24)$$

Substituting the value of β from eq. 24 in the eq. 4 yields:

$$\frac{e_k}{e_0} = \frac{1}{\hat{l}} \cdot \frac{(\hat{l}-1)^2}{(\hat{l}+1)^2} . \qquad \dots (25)$$

The point of maximum energy is obtained by deriving the above expression with regard to $\hat{l}$ and equating the result to zero, which yields:

$$\frac{\partial \frac{e_k}{e_0}}{\partial \hat{l}} = \frac{(\hat{l}-1)(\hat{l}^2-4\hat{l}-1)}{\hat{l}^2 (\hat{l}+1)^3} = 0 , \qquad \dots (26)$$

Which for $\hat{l} \neq 0$ solves for

$$\hat{l}_{cr} = 2 + \sqrt{5} \approx 4.2361 \qquad \dots (27)$$

$\hat{l}_{cr}$ could be expressed in terms of the Golden Ratio as:

$$\hat{l}_{cr} = 2 + \sqrt{5} = \frac{1+\Phi}{1-\Phi} = (1+\Phi)^3 \qquad \dots (28)$$

Notably, the resulting critical "stretch" is the "silver mean" [62-63], a number related to topologies of the Hausdorff dimension [64].

3.4 Wave Phase Transition and the Bose-Einstein Condensate

The body's wave energy as a function of the relative stretch is obtained substituting the value of β from eq. 24 in eq. 19, yielding:

$$\frac{e_w}{e_0} = \frac{2\left(\frac{\hat{l}-1}{\hat{l}+1}\right)^3}{1+\left(\frac{\hat{l}-1}{\hat{l}+1}\right)} = \frac{(\hat{l}-1)^3}{\hat{l}(\hat{l}-1)^2} \qquad \qquad ....\,(29)$$

The matter and wave energies as functions of the relative stretch $\hat{l}$ are depicted in Figure 5.

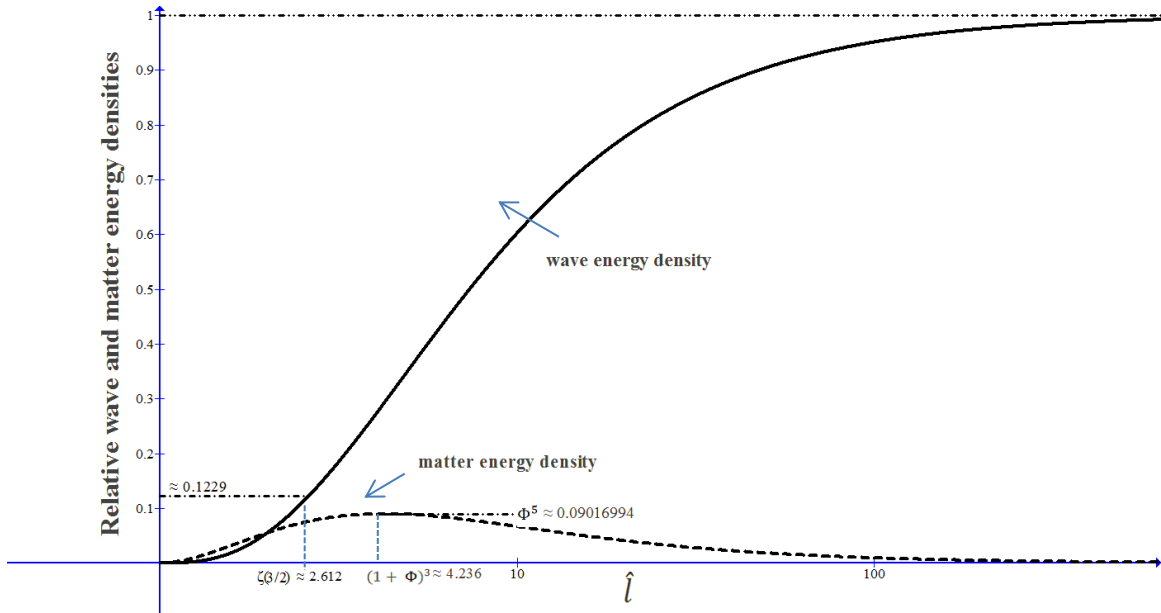**Figure 5**: e_m and e_w as functions of stretch $\hat{l}$

The figure reveals that the normalized wave energy $\frac{e_w}{e_0}$ increases rather sharply with the stretch $\hat{l}$, and then levels relatively slowly, approaching 1 as $\hat{l} \to \infty$. The turning point of the function's slope could be found by deriving e_w in eq. 29 with respect to $\hat{l}$ twice, and equating the result to zero, yielding:

24

$$\frac{\partial^2 e_w}{\partial \hat{l}^2} = \frac{2 \left(5 \hat{l}^4 - 16 \hat{l}^3 + 6 \hat{l}^2 + 4\hat{l} + 1\right)^3}{\hat{l}^3 \left(\hat{l}+1\right)^4} \; e_0 = 0 \qquad \qquad \text{.... (30)}$$

For $\hat{l} > 1$ we get:

$$5 \hat{l}^4 - 16 \hat{l}^3 + 6 \hat{l}^2 + 4\hat{l} + 1 = 0, \qquad \qquad \text{.... (31)}$$

Which solves for:

$$\hat{l}_{cr} = \frac{1}{15} \left(11 + \sqrt[3]{2906 - 90\sqrt{113}} + \sqrt[3]{2906 + 90\sqrt{113}}\right) \approx 2.612139 \approx \zeta(\tfrac{3}{2}) \quad \text{.. (32)}$$

Where ζ is the Riemann zeta function [65-66].

Thus, the critical stretch at which the wave energy density undergoes a "second order" phase transition is predicted to occur at stretch $\hat{l}_{cr} \approx 2.612375 \approx \zeta(\tfrac{3}{2})$. Strikingly, this result is identical to the critical de Broglie wave-length in connection with the critical temperature Tc for the formation of a Bose-Einstein condensate [67-68]. As it is well known, in the framework of de Broglie's wave-particle model, the statistical quantum mechanical analysis yields a critical de Broglie wave-length given by:

$$\lambda_{dB} = \left(\frac{2\pi\hbar^2}{mT_cK_B}\right)^{\frac{1}{2}} = \zeta\left(\frac{3}{2}\right) \qquad \qquad \text{.... (33)}$$

Where m is the particle's atomic mass m, Tc is the critical temperature, K_B is Boltzmann Constant, and $\hbar$ is the reduced Planck's constant. From equations 32 and 33 we can write:

$$e_{w_{cr}} = \frac{\left(\hat{l}_{cr}-1\right)^3}{\hat{l}_{cr}\left(\hat{l}_{cr}-1\right)^2} \; e_0 \approx 0.1229 \; e_0 \qquad \qquad \text{.... (34)}$$

3.5 Quantum Entanglement

According to quantum theory, entanglement between observables in two separate systems implies the existence of global states of composite systems that cannot be written as a product of the states of individual subsystems [48, 69-70]. For example, one can prepare two particles in a single quantum state such that when one is observed to be spin-up, the other one will always be observed to be spin-down and vice versa. As a result, measurements performed on one system seem to be instantaneously influencing other systems entangled with it, even when the systems are at large distances from each other.

In the following we show entanglement could be accounted for by the causality of spatial locality. For demonstration we treat here a simple EPR bipartite system comprised of two identical particles moving away from each other with constant linear velocity. Suppose that at $t = t_0 = 0$ the two particles are distanced from each other, such that particle A moves leftward (in -x direction) toward Alice's box, while the particle B is moving rightward (in +x direction) toward Bob's box (see Figure 6).

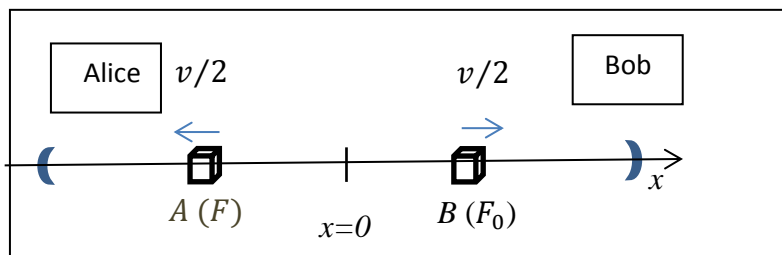**Figure 5**: Illustration of an EPR-type experiment

For a relative distancing velocity $\beta = \frac{v}{v_c}$, the relative length "stretch" of particle B in the frame of reference of particle A is given by eq. 2, that is: $l/l_0 = \dfrac{1+\beta}{1-\beta}$, and its relative mass density from eq.

3 is given by: $\rho/\rho_0 = \dfrac{1+\beta}{1-\beta}$. These relationships are depicted in Figure 6.
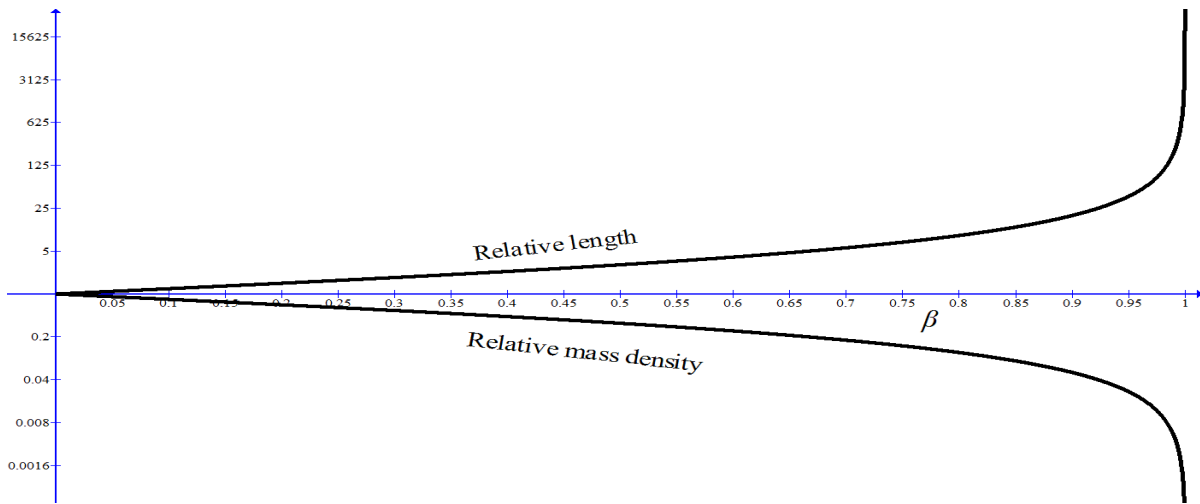
Figure 6. Relative length and mass density as functions of velocity

The above results could be summarized as follows: when a particle is distanced from another particle with velocity v, it will incur a relativistic "stretch" in the rest frame of the other particle, and the amount of stretch will depend on the relative velocity as described by eq. 2 (see Figure 6). Concurrently, the particle's total rest mass m_0 will be distributed along the stretched length and its mass density along the travel path will be diminished (see eq. 3 and Figure 6). The rates of stretching in distance and decrease in density will always balance, such that the total rest mass of the body remains unchanged. Note that the state of affairs described above is consistent with de Broglie's wave-particle model. In general, at high-enough velocities, β, a distancing particle with respect to a rest frame of reference will gradually abandon its matter properties and behave more like a wave packet. Similarly, wave quanta that are forced to decelerate will eventually reach a point of phase transition, after which it will behave more like a particle than a wave. Put simply, in the framework of Epistemic Relativity, waves could be considered extremely stretched matter, whereas matter could be viewed as extremely crunched waves.

The cross correlation between the two energy densities of particles A and B for a given relative velocity β, over the dimension of motion, could be calculated as:

27

$$r(\hat{l}) = e_k * e_0 = \int_{\hat{l} \geq 1} e_k(\xi) \, e_0(\xi + \hat{l}) \, d\hat{l} = \ln\left(\frac{\hat{l}+1}{\hat{l}}\right) - \frac{4}{(\hat{l}+1)(\hat{l}+2)} \quad . \qquad \dots (35)$$

Maximum correlation is obtained at $\hat{l}$ satisfying $\frac{\partial(e_k * e_0)}{\partial \hat{l}} = 0$, which yields:

$$- \hat{l}^3 + 3\,\hat{l}^2 + 4\,\hat{l} - 4 = 0 \, , \qquad\qquad\qquad\qquad \dots (36)$$

Which for $\hat{l} \geq 1$, solves at $\hat{l} \approx 3.7785$.

Substitution in eq. 35 gives $r_{max} \approx 0.08994$.

4. Application to Intergalactic Cosmology

In applying our epistemic model for investigating the intergalactic universe, several simplifications assumptions are made: 1. that the universe is isotropic, 2. that each galaxy could be represented by a lumpy point mass, and 3. that intergalactic interactions are weak and thus negligible. The isotropy assumption concurs with the "cosmological principle" and with abundant observations indicating that the universe looks the same in all directions. The second and third assumptions are justified by the gigantic number of galaxies in the observable universe, estimated to be ~100 billion galaxies and the enormous (and continually increasing) distances between galaxies. Obviously, the present simplified model fits better for describing the dynamics of more distant galaxies from an observer on Earth. We know for example that the Milky Way and the smaller galaxy Andromeda are continually attracted to each other, and that Andromeda will be eventually sucked by our home galaxy.

4.1. Recession velocity

Given the above simplification, we consider an observer on Earth who conducts measurements of an event taking place on a distant galaxy which during the measurement recedes from the observer's reference frame with uniform velocity v. Assume that the event is associated with the emission of light or another wave with similar velocity c, and that the observer on earth measures the time duration of the event by means of the signals emitted from the galaxy in which the event has taken

place. Using Eq. 1 together with the classical Doppler formula, it is shown in [71] that the arriving

waves red-shift z, due to the body's recession at velocity $\beta = \frac{v}{c}$ is given by:

$$z = \frac{\beta}{1-\beta} \qquad\qquad ….. (37)$$

And the transverse relationship is:

$$\beta = \frac{z}{1+z} \qquad\qquad ….. (38)$$

The comparable expression of SR is:

$$\beta = \frac{(1+z)^2 - 1}{(1+z)^2 + 1} \qquad\qquad ….. (39)$$
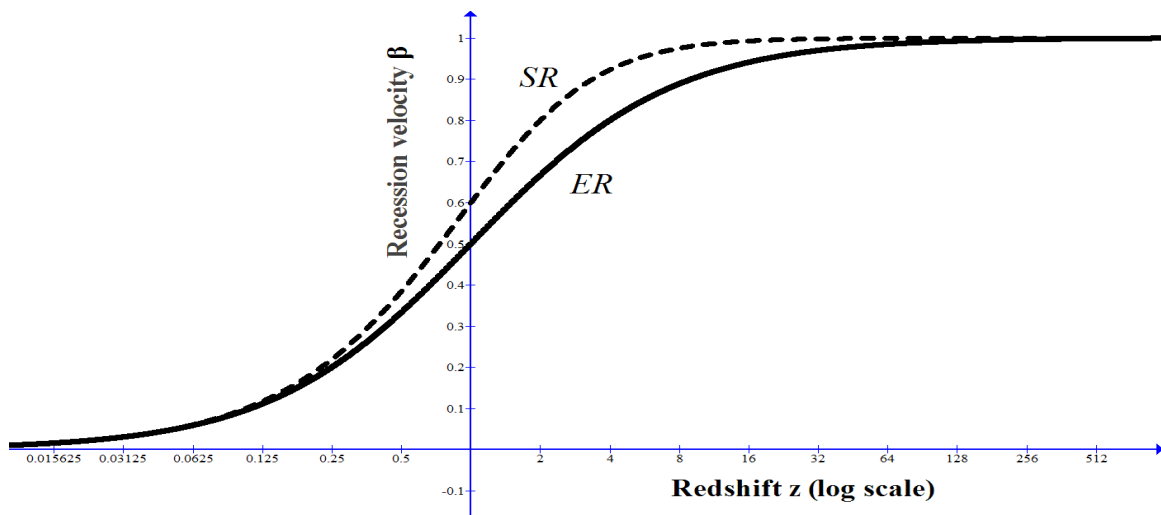

Figure 7. Predicted recession velocity as a function of redshift z

Figure 7 depicts Epistemic Relativity 's prediction of the universe's *recession velocity* with respect to

an observer on earth as function of the redshift *z*. The dashed line depicts the comparable prediction

of SR. The qualitative resemblance between the predictions of the two theories is easily noticeable.

Roughly speaking, Epistemic Relativity predicts that for very high redshifts (from z ~ 8 to z ~ 1089),

the recession velocity is close to the velocity of light, and its deceleration rate is low and relatively

steady. This prediction confirms with the well accepted inflation theory [72-74] predicting an early

period of accelerated expansion of the universe. For very low redshifts ($z \leq 0.1$), the recession velocity is very low, and its deceleration rate is low and relatively steady. The epoch spanning from $z \sim 1089$ to $z \sim 8$ likely corresponds to the time of massive galaxy formation in the early universe, whereas the epoch of very low redshifts ($z < 0.1$) corresponds to the time of young stars and galaxy formations. In the midrange of redshifts, between $z \sim 8$ and $z \sim 0.1$, the universe underwent a period of rapid deceleration.

4.2. Kinetic Energy

To further investigate the cosmology constructed by Epistemic Relativity theory, we use the relationship between recession velocity and redshift (eq. 38) to express the transformation depicted in Table 1 in terms of redshift. Simple calculations yield the results depicted in Table 4.

As the table shows Epistemic Relativity prescribes that relativistic time and distance stretch linearly with redshift, while the "dilution" in mass density is hyperbolic with z. Far more interesting is the dependence of relativistic kinetic energy density on redshift depicted by the continuous line in Figure 8. The dotted line in the figure depicts the relativistic "loss" in the observed kinetic energy density, defined as $\frac{e_N - e_k}{e_0}$, where $e_0 = \frac{1}{2} \rho_0 c^2$, and e_N is the classical Newtonian term of kinetic energy per mass density of ρ_0. For shall call this term hereafter "unobservable" or "dark" energy. Strikingly, the distribution of the kinetic energy in the universe is predicted to be bell shaped, with quite unexpected, yet fascinating symmetries: It is centered at redshift equaling the Golden Ration, $z = \frac{\sqrt[2]{5}+1}{2} = \varphi \approx 1.618$, with maximum equaling $(\frac{1}{\varphi})^5 \approx 0.09016994$.

Table 4

Epistemic Relativity Transformations in terms of Redshift z

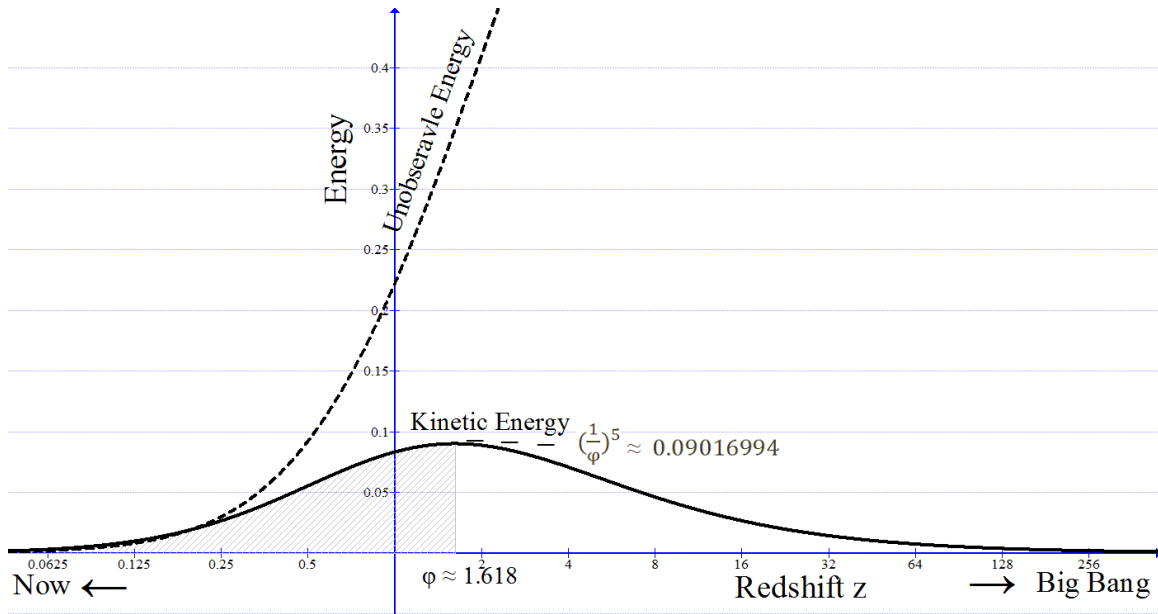| Physical Term	Relativistic Expression	
Time	$\dfrac{t}{t_0} = z + 1$	(40)
Distance	$\dfrac{x}{x_0} = 2z + 1$	(41)
Mass density	$\dfrac{\rho}{\rho_0} = \dfrac{1}{2z+1}$	(42)
Kinetic energy density	$\dfrac{e_k}{e_0} = \dfrac{z^2}{(z+1)^2(2z+1)}$	(43)

Figure 8: Densities of kinetic and unobservable energies as functions of redshift z

These results could be verified by deriving the term in Eq. 43 with respect to z and equating the result to zero:

$$\frac{d}{dz}\left(\frac{z^2}{(z+1)^2(2z+1)}\right) = \frac{2z\,(-z^2+z+1)}{(z+1)^3(2z+1)^2} = 0 \qquad \dots\ (44)$$

For $z \neq 0$, we have

$$z^2 - z - 1 = 0 \qquad \dots\dots\ (45)$$

Or

$$z_{max} = \frac{\sqrt[2]{5}+1}{2} = \varphi \approx 1.618 \qquad \dots\ (46)$$

Where φ is the Golden Ratio.

The corresponding max value of $\frac{e_k}{e_0}$ is equal to:

$$\frac{e_k}{e_0} = \frac{1-(\varphi-1)}{1+(\varphi-1)}(\varphi-1)^2 = \frac{1-(\varphi-1)}{\varphi}(\varphi-1)^2 \qquad \dots(47)$$

Using the relationship $\varphi - 1 = \frac{1}{\varphi}$, we get

$$\frac{e_k}{e_0} = \left(\frac{1}{\varphi}\right)^5 \approx 0.09016994 \qquad \dots\ (48)$$

The corresponding recession velocity at $z = \varphi$ is:

$$\beta = \frac{\varphi}{\varphi+1} = \varphi - 1 \approx 1.618 - 1 = 0.618 \qquad \dots\ (49)$$

The physical meaning of the above results could be described as following: For an observer on Earth, the relativistic kinetic energy density is predicted to increase with redshift up to redshift z ~ 1.618, at which its reaches its maximum value equaling ≈ 0.09016994. This value is quall, to the eighth decimal digit, to L. Hardy's probability of entanglement [18]. From $z = 0$ to $z \approx 1.618$ (recession velocity β between zero and ≈ 0.618) galactic bodies are predicted to exhibit a quasi-classical

32

behavior. That is, despite continuous depreciation in kinetic energy density relative to the classical Newtonian value, more recession velocity is still associated with higher energy density. Starting from the critical kink point at z ≈ 1.618, galactic bodies are predicted to undergo a relativistic phase transitions, after which the classical monotonous increase in kinetic energy with velocity (and redshift) is converted, such that higher recession velocities (higher redshift) are associated with lower, rather than higher kinetic energy density. The apparent energy "loss" is contained in an unobservable or "dark" form (see figure 8), such that the total energy is conserved.

The resemblance between the predicted non-monotonicity of normal energy density with redshift, and the well-known GZK cutoff limit could not be overlooked. In their well-known papers, Greisen [75], and Zatsepin and Kuzmin [76], proposed an upper limit to the cosmic-ray energy spectrum. A first observation of the Greisen-Zatsepin-Kuzmin suppression was reported in the High Resolution Fly's Eye (HiRes) experiment [77]. HiRes measurement of the flux of ultrahigh energy (UHE) cosmic rays showed a sharp suppression at an energy of 6×10^{19} eV, consistent with the expected cutoff energy. Interestingly, in the HiRes experiment the evolution of QSO's and AGN's has been measured and both types of source show a break in their luminosity densities at about z=1.6, quite consistent with the Golden Ratio prediction of z ≈ 1.618. Strong support to the maximal energy density at z ≈ 1.618 has been reported by numerous discoveries of quasars, galaxies, and AGNs, indicating a break in luminosity densities at about z=1.6 (e.g., [78-79]), including a recent discovery of galaxies at redshift equaling exactly 1.618 [80].

However, it is also known that several experiments (e.g., [81-82]) have reported the detection of one event each above 10^{20} eV, and a continuing, unbroken energy spectrum beyond the predicted GZK threshold was later reported by a larger experiment, the Akeno Giant Air Shower Array (AGASA) [83-84]. These seemingly contradicting results are reconciled by the cosmology of Epistemic Relativity, as could be directly verified from the relativistic kinetic energy density depicted in Figure 8.

4.3. Dark Energy

Background

One of the big challenges facing modern cosmology pertains to the nature of dark energy. No existing theory is capable of explaining what dark energy is, but it is widely believed that it is some unknown substance with an enormous anti-gravitational force (negative energy), which drives the galaxies of our universe apart. Despite efforts to ascribe the theoretical discovery of dark energy to Einstein's cosmological constant λ, the reference to λ in current ΛCDM cosmologies is no more than metaphoric. In fact, adherence to general relativity requires that for $\lambda \neq 0$, its magnitude should be ≈ 10^{120} (!) times the measured ratio of pressure to energy density [85]. An alternative explanation argues that dark energy is an unknown dynamical fluid, namely, one with a state equation that is dynamic in time. This type of explanation is represented by theories and models that differ in their assumptions regarding the nature of the state equation dynamics [86–88]. This explanation is no less problematic, because it entails the prediction of new particles with masses 35 orders of magnitude smaller than the electron mass, which might imply the existence of new forces in addition to gravity and electromagnetism [85]. At present, no persuasive theoretical explanation accounts for the existence, dynamics, and magnitude of dark energy and its resulting acceleration of the universe.

Prediction

In Epistemic Relativity theory, the cosmic unobservable (or dark) energy density at a given recession velocity (redshift) is defined here as the *energy "loss" due to relativity*, or:

$$e_d(\beta) = \frac{1}{2}\rho_0{}^2 v^2 - \frac{1}{2}\rho_0{}^2 c^2 \frac{(1-\beta)}{(1+\beta)}\beta^2$$

$$= \frac{1}{2}\rho_0{}^2 c^2 \beta^2 \left(1 - \frac{(1-\beta)}{(1+\beta)}\right) = \frac{1}{2}\rho_0{}^2 c^2 \frac{2\beta^3}{(1+\beta)} \qquad \text{... (50)}$$

And:

$$\frac{e_d(\beta)}{e_0} = \frac{2\beta^3}{(1+\beta)} \qquad \text{.... (51)}$$

Where β is the recession velocity with respect to an observer on Earth. In terms of redshift, the above equation becomes:

$$\frac{e_d(z)}{e_0} = \frac{2z^3}{(z+1)^2(2z+1)} \qquad \qquad \dots(52)$$

It is important to stress that Epistemic Relativity's interpretation of unobservable (dark) energy has nothing to do with the current belief holding that dark energy is some sort of unknown *negative* energy that is responsible to the accelerating recession of the universe.

The redshift at which the densities of kinetic and "dark" energy densities are predicted to be equal is obtained from solving the equation $e_k(z) = e_d(z)$, or:

$$\frac{z^2}{(z+1)^2(2z+1)} = \frac{2z^3}{(z+1)^2(2z+1)} \qquad \qquad \dots (53)$$

Yielding

$$z = \frac{1}{2} \ (\text{or } \beta = \frac{1}{3}) \qquad \qquad \dots (54)$$

Figure 9 depicts the ratios of the two energy densities $\frac{e_k(z)}{e_0}$ and $\frac{e_d(z)}{e_0}$ as functions of redshift. As shown in the figure Epistemic Relativity predicts that kinetic and "dark" energies mirror image each other around an axis of symmetry $\frac{e_k(z)}{e_0} = \frac{e_d(z)}{e_0} = 0.5$, such that kinetic energy dominates the universe only from now up to redshift $z = \frac{1}{2}$, while dark energy dominating the rest of the universe from $z > 0.5$ the Big Bang era.
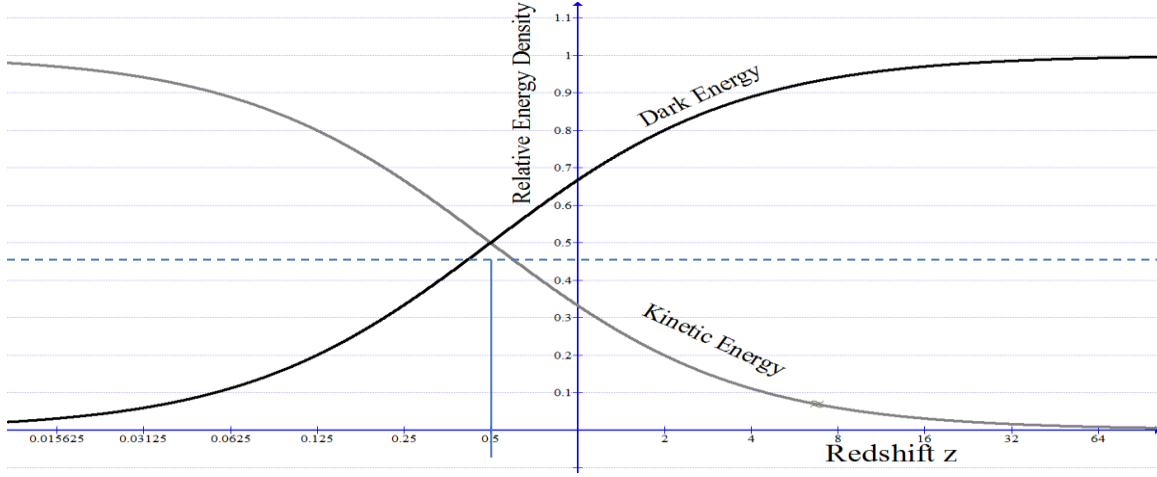
Figure 9. The ratios of the kinetic and dark energy densities as a function of redshift

4.4 Comparison with ΛCDM cosmologies

To compare the theory's predictions with observationally based ΛCDM cosmologies, we calculated the total normal and dark energy densities for any redshift range (z_1, z_2), $z_2 > z_1$. The results are respectively:

$$\frac{e_k(z_1 - z_2)}{e_0} = \int_{z_1}^{z_2} \frac{e_k(z)}{e_0} \, dz = \int_{z_1}^{z_2} \frac{z^2}{(z+1)^2(2z+1)} \, dz = \frac{1}{2} \ln\left(\frac{2z_2+1}{2z_1+1}\right) - \frac{z_2-z_1}{(z_2+1)(z_1+1)} \quad \dots (55)$$

and

$$\frac{e_d(z_1 - z_2)}{e_0} = \int_{z_1}^{z_2} \frac{e_d(z)}{e_0} \, dz = \int_{z_1}^{z_2} \frac{2z^3}{(z+1)^2(2z+1)} \, dz$$

$$= (z_2 - z_1) + 2\frac{(z_2-z_1)}{(z_2+1)(z_1+1)} - 2\ln\left(\frac{(z_2+1)}{(z_1+1)}\right) - \frac{1}{2}\ln\left(\frac{(2z_2+1)}{(2z_1+1)}\right) \quad \dots(56)$$

We tested the above results using data from Wittman et al. (2000) [89] who reported the detection of cosmic shear using 145,000 galaxies, at redshift ranging between 1 to 0.6, and along three separate lines of sight. The analysis was based on weak lensing data from COBE and on galaxy clusters. The study concluded the dark matter is distributed in a manner consistent with either an open universe, with $\Omega_b = 0.045$, Ω_{matter} - $\Omega_b = 0.405$, $\Omega_\Lambda = 0$, or with a ΛCDM with $\Omega_b = 0.039$, Ω_{matter} - $\Omega_b =$

36

0.291, $\Omega_\Lambda = 0.67$, where Ω_b is the fraction of critical density in ordinary (baryonic) matter, Ω_{matter} is the fraction of all matter, and Ω_Λ is the fraction of dark energy. In the open universe model, we have $\Omega_{matter} = 0.045 + 0.405 = 0.45$, and $\Omega_\Lambda = 0$, whereas in the ΛCDM, we have $\Omega_{matter} = 0.039 + 0.291 = 0.33$, and $\Omega_\Lambda = 0.67$. To test the prediction of Epistemic Relativity, we calculated the ratios of kinetic and dark energies in redshift range from $z_1=0.6$ to $z_2=1$, by substitution in equations 55 and 56, respectively, yielding:

$$\frac{e_k(0.6-1)}{e_0} = \frac{1}{2}\ln\left(\frac{2+1}{2 \times 0.6+1}\right) - \frac{1-0.6}{(1+1)(0.6+1)} = \frac{1}{2}\ln\left(\frac{3}{2.2}\right) - \frac{0.4}{3.2} \approx 0.0301 \qquad \text{...... (57)}$$

and

$$\frac{e_d(0.6-1)}{e_0} = (1-0.6) + 2\frac{(1-0.6)}{(1+1)(0.6+1)} - 2\ln\left(\frac{1+1}{0.6+1}\right) - \frac{1}{2}\ln\left(\frac{2+1}{2 \times 0.6+1}\right)$$

$$= 0.4 + \frac{0.8}{3.2} - 2\ln\left(\frac{2}{1.6}\right) - \frac{1}{2}\ln\left(\frac{3}{2.2}\right) \approx 0.0486 \qquad \text{..... (58)}$$

Thus, the ratios of e_k and e_d in $z = 0.6 \rightarrow 1$ are:

$$\frac{e_k}{e_{tot}} = \frac{e_k}{e_k+e_d} = \frac{0.0300775}{0.0300775 + 0.0486354} \approx 0.382 \ (\approx 38.2\%) \qquad \text{.... (59)}$$

And:

$$\frac{e_d}{e_{tot}} = \frac{e_d}{e_k+e_d} = \frac{0.0486354}{0.0300775+0.0486354} \approx 0.618 \ (\approx 61.8\%) \qquad \text{.... (60)}$$

Which is in agreement with the observations based ΛCDM model with ($\Omega_m = \frac{1}{3}$, $\Omega_\Lambda = \frac{2}{3}$).

Calculation of the ratios of normal and dark energy in the range spanning from now ($z_1=0$) to the critical redshift $z_2 = \varphi \approx 1.618$ yields:

$$\frac{e_k(0-\varphi)}{e_0} = \frac{1}{2}\ln(2\varphi + 1) - \frac{\varphi}{(\varphi+1)} \approx 0.1038 \qquad \text{.... (61)}$$

And:

$$\frac{e_k(0-\varphi)}{e_0} = \varphi+2\frac{\varphi}{\varphi+1} - 2\ln(\varphi+1) - \frac{1}{2}\ln(2\varphi) \approx 0.3420 \qquad \text{....(62)}$$

Thus we have,

$$\frac{e_k}{e_k+e_d} = \frac{0.138}{0.138+0.3420} \approx 0.233 \text{ (or 23\%)} \qquad \text{.... (63)}$$

And

$$\frac{e_d}{e_k+e_d} = \frac{0.3420}{0.138+0.3420} \approx 0.767 \text{ (or 76.7\%)} \qquad \text{.... (64)}$$

Notably, the above prediction is in excellent agreement with the ΛCDM cosmology with $\Omega_{matter} = 0.23$, $\Omega_{\Lambda} = 0.77$ (see, e.g., [90-92]), and quite close to the $\Omega_{matter} = 0.26$, $\Omega_{\Lambda} = 0.74$ cosmology (see, e.g., [93-95]).

Equations 55 and 56 can be used to put constraints of future observations based cosmologies. For example, for a cosmology that best fits the entire range from $z = 0$ to $z = 8$, we have:

$$\frac{e_k(0-8)}{e_0} = \frac{1}{2}\ln(17) - \frac{8}{9} \approx 0.5277 \qquad \text{.... (65)}$$

And

$$\frac{e_k(0-8)}{e_0} = 8 + \frac{16}{9} - 2\ln(9) - \frac{1}{2}\ln(17) \approx 3.9967 \qquad \text{.... (66)}$$

And the predicted ratios of kinetic and dark energies are, respectively,

$$\frac{e_k}{e_{tot}} = \frac{e_k}{e_k+e_d} = \frac{0.5277}{0.5277+3.9967} \approx 0.12 \text{ (12\%)} \qquad \text{.... (67)}$$

And

$$\frac{e_d}{e_{tot}} = \frac{e_d}{e_k+e_d} = \frac{3.9967}{0.5277+3.9967} \approx 0.88 \text{ (88\%)} \qquad \text{.... (68)}$$

5. Application to Gravitational Black Holes

5.1 Background

The term "black hole" was coined by John Wheeler in 1964, but the possibility of its existence within the framework of Newtonian physics was conjectured by John Michell in 1784, who argued for the possible existence of an object massive enough to have an escape velocity greater than the velocity of light [96]. Twelve years later, Simon Pierre La Place also predicted the existence of black holes. Laplace argued that "It is therefore possible that the largest luminous bodies in the universe may, through this cause, be invisible" [97].

A better understanding of black holes, and how gravity and waves intermingle, had to wait until 1915, when Albert Einstein delivered a lecture on his theory of General Relativity (GR) to the German Academy of Science in Berlin. Within a month of the publication of Einstein's work, Karl Schwarzschild, while serving in the German Army on the Russian front, solved Einstein's field equations for a non-rotating, uncharged, spherical black hole [98]. For a star of a given mass, M, Schwarzschild found the critical radius R = $\frac{2\,G\,M}{c^2}$, where G is the gravitational constant and c is the velocity of light, at which light emitted from the surface would have an infinite gravitational redshift, and thereby infinite time dilation. Such a star, Schwarzschild concluded, would be undetectable by an external observer at *any* distance from the star.

Our understanding of the processes involved in the evolution and decay of black holes is largely due to quantum mechanical and thermodynamic theories. Early in 1974, Stephen Hawking predicted that a black hole should radiate like a hot, non-black ("gray") body [99]. Hawking's theory of black holes, is consistent with Bekenstein's generalized second law of thermodynamics [100], stating that the sum of the black-hole entropy and the ordinary thermal entropy outside the black hole cannot decrease. According to this prediction, black holes should have a finite, non-zero, and non-decreasing temperature and entropy.

The first X-ray source, widely accepted to be a black hole, was Cygnus X-1 [101]. Since 1994, The Hubble Space Telescope, and other space-crafts and extremely large ground telescopes (see, e.g., [102-103], have detected numerous black holes of different sizes and redshifts. We now know that black holes exist in two mass ranges: small ones of (M ≲ 10 M⊙) (M⊙, solar mass), believed to be the evolutionary end points of the gravitational collapse of massive stars, and supermassive black holes of M ≳ 10^6 M⊙, responsible for the powering of quasars and active galactic nuclei (AGN) [104-106]. Supermassive black holes, residing at the centers of most galaxies, are believed to be intimately related to the formation and evolution of their galaxies [104- 108].

5.2 Pathology and Previous Solutions

As mentioned above, the solution to Einstein's field equations [98-99] yields a critical hole radius of R = $\frac{2\,GM}{c^2}$. However, Schwarzschild's solution suffers from a serious pathology, because it predicts a singularity whereby the fabric of spacetime is torn, causing all matter and radiation passing the event horizon to be ejected out to an undefined spacetime, leaving the black hole empty, thus, in violation of the laws of thermodynamics and contradiction with quantum mechanics [e.g., 99-100]. Many believe that the black holes (and the Big Bang) singularities mark a breakdown in GR.

Attempts to solve the singularity problem are aplenty. Bardeen was the first to propose a regular black hole model [109]. In 1968, he produced a famous model, conventionally interpreted as a counterexample to the possibility that the existence of singularities may be proved in black hole spacetimes without assuming either a global Cauchy hyper-surface or the strong energy condition. Other regular "Bardeen black holes" models have been also proposed [e.g., 110-115], but none of these models is an exact solution to Einstein equations [116]. Other solutions to produce singularity-free black hole come from string theory (e.g., [117-118]), and quantum mechanics [e.g., 119-123]. As examples, Ashtekar and others [120-121] proposed a loop quantum gravity model that avoids the singularities of black holes and the Big Bang. Their strategy was to utilize a regime that keeps GR intact, except at the singularity point, at which the classical spacetime is bridged by a discrete

quantum one. Although the solution is mathematically difficult, its strategy is simple. It begins with semi-classical state at large late times ("now"), and evolves it back in time, while keeping it semi-classical until one encounters the deep Planck regime near the classical singularity. In this regime, it allows the quantum geometry effects to dominate. As the state becomes semi-classical again on the other side, the deep Planck region serves as a quantum bridge between two large, classical spacetimes [119].

5.3 Prediction of the black hole radius

Figure 10 depicts a schematic representation of a supermassive black hole with mass M and radius R residing at the center of its host galaxy.
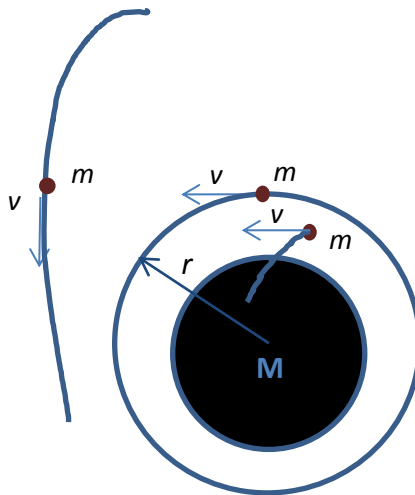

Figure 10. Three particles near a black hole

The figure shows three particles, with equal masses and velocities, at different distances from the center of the black hole. As depicted in the figure, the more distant particle will be deflected toward the black hole, but will escape it due to its large distance, and continue its travel in space. By contrast, the closest particle to the black hole will experience a strong enough gravitational force to cause its absorption into the black hole. Now consider the third particle, which rotates around the black hole at radius r. Such particle could be a baryon or wave quanta entrapped at a critical distance,

ensuring that it rotates around the black hole. For such particle, the acceleration $|\vec{a}|$ supporting a uniform radial motion with radius r should satisfy

$$a = |\vec{a}| = \frac{v^2}{r} = \frac{c^2}{r} \beta^2 \qquad \dots (69)$$

The force supporting such motion, according to Newton's second law, could be expressed as:

$$F = \frac{\partial P}{\partial t} = \frac{\partial (mv)}{\partial t} = m \frac{\partial (v)}{\partial t} + v \frac{\partial (m)}{\partial t}$$

$$= m\, a + v \frac{\partial (m)}{\partial v} \frac{\partial (v)}{\partial t} = m\, a + v\, a\, \frac{\partial (m)}{\partial v} = \left(m + v \frac{\partial (m)}{\partial v}\right) a \qquad \dots (70)$$

Substitution the term for m from Eq. 3 in Table 1, and deriving m with respect to v yields:

$$F = \frac{1 - 2\beta - \beta^2}{(1+\beta)^2} \, m_0 \, a \qquad \dots (71)$$

Substitution the value of a, from Eq. 69 in Eq. 71 yields:

$$F = \frac{1 - 2\beta - \beta^2}{(1+\beta)^2} \, m_0 \, a = \frac{1 - 2\beta - \beta^2}{(1+\beta)^2} \, m_0 \, \frac{v^2}{r} = m_0 \, c^2 \, \frac{1 - 2\beta - \beta^2}{(1+\beta)^2} \, \beta^2 \, \frac{1}{r} \qquad \dots (72)$$

Using Newton's general law of gravitation, we get:

$$G \frac{m_0 \, M}{r^2} = m_0 \, c^2 \, \frac{1 - 2\beta - \beta^2}{(1+\beta)^2} \, \beta^2 \, \frac{1}{r} \qquad \dots (73)$$

Solving for r yields:

$$r = \frac{G\,M}{c^2} \, \frac{(1+\beta)^2}{1 - 2\beta - \beta^2} \, \beta^2 \qquad \dots (74)$$

Assuming spherical symmetry, eq. 74 describes the dynamics of the host galaxy as a function of velocity. For a light photon ($\beta = 1$), we have:

$$r\,((\beta = 1) = R = \frac{2\,G\,M}{c^2} \qquad \dots (75)$$

Which exactly equals the Schwarzschild radius, *but with no singularity in the hole's interior.* Interestingly, the solution (eq. 74) has a naked *spatial* singularity at β satisfying:

$$1 - 2\beta - \beta^2 = 0 \qquad\qquad\qquad\qquad\qquad .... (76)$$

Solving for β, we have:

$$\beta = \sqrt[2]{2} - 1 \approx 0.4142 \qquad\qquad\qquad\qquad\qquad ..... (77)$$

With corresponding redshift of $z = \frac{\beta}{1-\beta} = \frac{1}{\sqrt[2]{2}} \approx 0.707$.

It is important to stress that the predicted singularity is in space and not in spacetime, as prescribed by the Schwarzschild's solution of General Relativity's field equations. In fact, Newtonian Relativity in general, including in its present application to the black hole problem, does not require reference to the notion of spacetime. To express the derived radius in terms of redshift, we substitute the value of β from Eq. 38 in Eq. 74 and solve for r, yielding:

$$r = \left(\frac{G\,M}{c^2}\right) \frac{z^2(1+2z)^2}{(1+z)^2\,(1-2z^2)} \qquad\qquad\qquad .... (78)$$

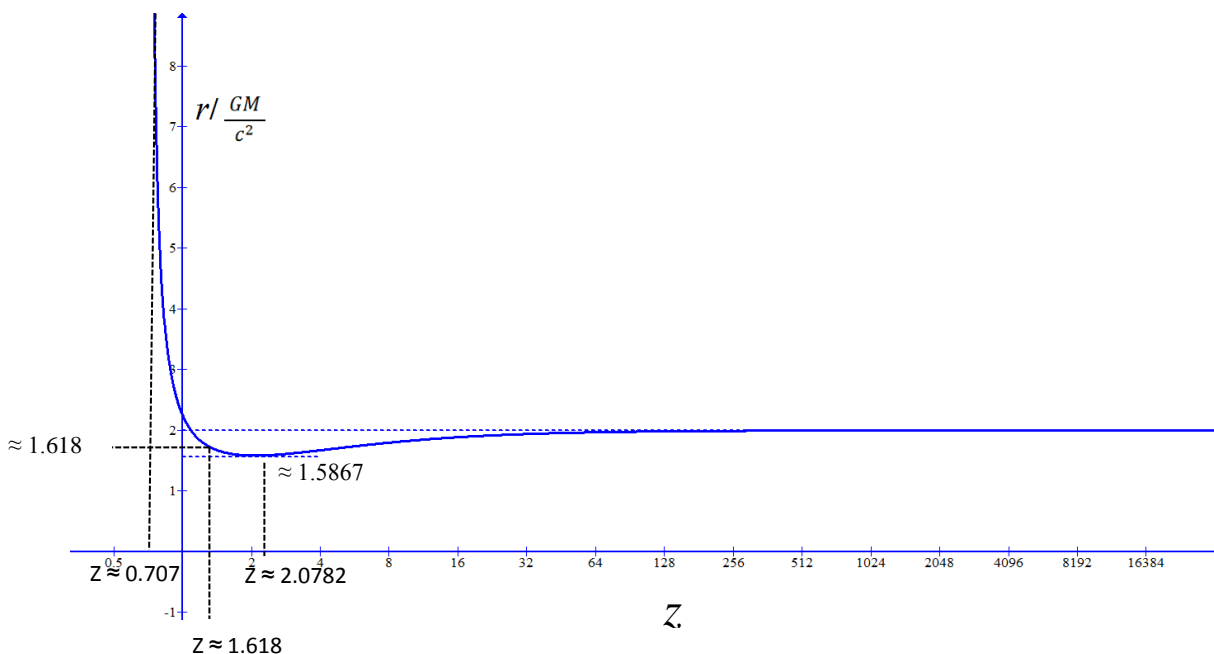Figure 11 depicts the ratio r, normalized by $\frac{GM}{c^2}$, as a function of z.

Figure 11. $r / \left(\frac{GM}{c^2}\right)$ as a function of redshift

As shown by the figure, for very high redshifts r converges to $2\frac{G\,M}{c^2}$ (the Schwarzschild radius).

Moreover, the result in Eq. 19 has some interesting properties. (1) r has a naked *spatial singularity*, at $z = \frac{1}{\sqrt[2]{2}} \approx 0.707$, (2) It displays a striking Golden Ration symmetry, such that for $z = \varphi \approx 1.618$, $r\ /$

$(\frac{G\,M}{c^2}) \approx 1.618$, (3) It has a point of minimum in the range between the above mentions redshifts. To find the point of minimum we derive $r\ /\ (\frac{G\,M}{c^2})$ with respect to z and equate the result to zero, yielding:

$$4\,z^4 - 2\,z^3 - 10\,z^2 - 6\,z - 1 = 0 \qquad\qquad \text{.... (79)}$$

Which solves at $z_m \approx 2.078$, yielding $r_m \approx 1.5867\ (\frac{G\,M}{c^2})$.

The prediction of an extreme galactic activity at $z \approx 0.707$ is supported by many observational studies, which reported the detection of quasars, blazars and other AGNs at $z \approx 0.707$ [e.g., 125-128]. For example, a recent study by Steinhardt et al. [125] reported the discovery of a Type 1 quasar, SDSS 0956+5128, with extreme velocity offsets at redshifts z = 0.690, 0.714, and 0.707. The prediction of AGNs at z ≈ 2.078 is also confirmed by observations (e.g. [128-129]).

We also compared the dynamical dependence of r on redshift (eq. 78) with the dynamics reported in [130] for a cosmology of $\Omega_M = 0.3$ and $\Omega_\Lambda = 0.7$, $H_0 = 70$ km s^{-1} Mpc^{-1}. Figure 12a depicts the predicted radius r (in Km) as a function of redshift for intermediate and massive black holes and Figure 12b depicts comparable results reported in [130]. Comparison of the two figures, despite differences in scaling, reveals a remarkable similarity between the results of the two models.
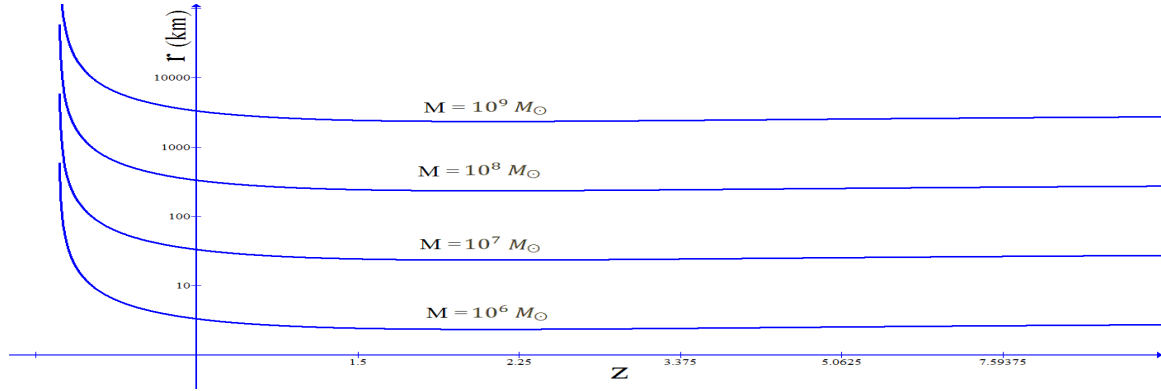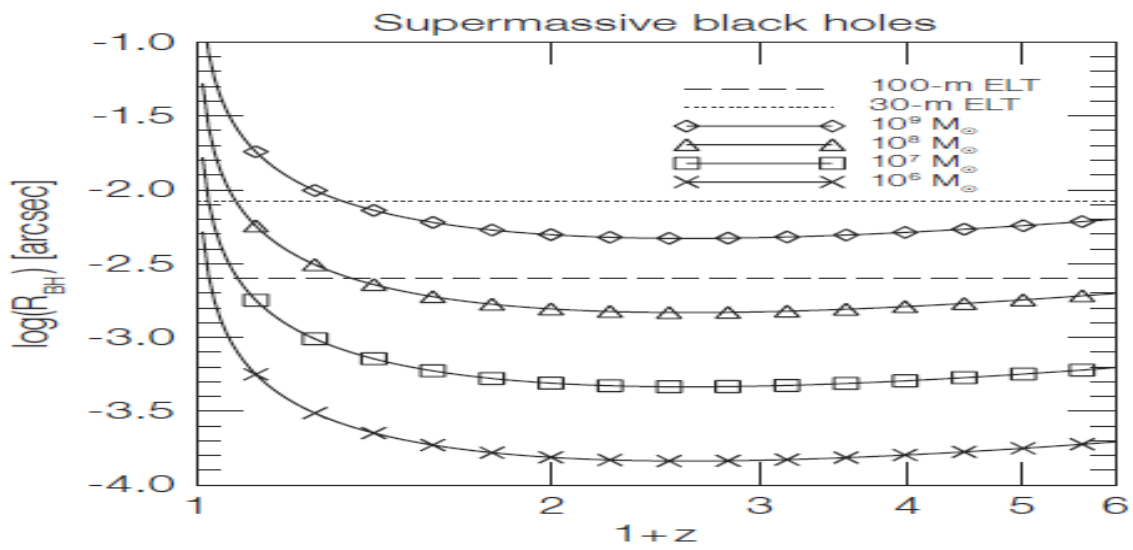
Figure 12a

Figure 12b

Figure 12. Predicted *r* as a function of *z* (Fig. 12a) and comparable results based on ΛCDM model ($\Omega_M = 0.3$, $\Omega_\Lambda = 0.7$, $H_0 = 70$ km s^{-1} Mpc^{-1}) reported by Hook (2005) [130] (Fig 12b).

6. Summary and Concluding Remarks

We considered an inertial physical system in which signals about physical measurements of time and other physical variables conducted in one reference-frame are transmitted to a receiver moving with relative constant velocity *v*, by an information carrier with a constant velocity v_c with respect to transmitter's rest-frame ($v_c > v$). Without making any further theoretical assumptions or putting constrains on the systems variables, derived relativistic time, distance, mass, and energy expressions,

relating measurements transmitted by the information sender to the corresponding information registered at the receiver. The derived relativistic distance expression violates the Lorentz principle for distancing bodies, by predicting length extension instead of contraction. This feature of the proposed model leads to the prediction that at sufficiently high normalized velocities, distanced bodies can maintain spatial locality, acting at each other proximally and not at a distance. In other words the model predicts that at sufficiently high velocities, distance bodies can get entangled physically.

Since the proposed model is *scale independent* with respect to the size of spatial dimension and mass of moving bodies, it is applicable without alterations or additions of free parameters for studying the dynamics of Nano particles and galactic structures. In the present article we demonstrated that the model accounts well for a multitude of phenomena and experimental findings. In the sector of elementary particles, the theory makes excellent predictions of the Michelson-Morley's "null" result, the relativistic lifetime of decaying Muons, the Sagnac effect, the neutrino velocities reported by OPERA and other collaborations, and more. Application of the model to cosmology, without alteration or addition of free parameters, yields successful accounts for several important cosmological findings, including the pattern of recession velocity predicted by inflationary theories, the amounts of matter and dark energy in various segments of redshift, reported in recent ΛCDM cosmologies, the GZK energy suppression phenomenon, and the radius of gravitational black holes, equaling the Schwarzschild radius ($R = \frac{2\,G\,M}{c^2}$), but without a troubling interior *singularity*. For the quantum sector we showed that the model, despite being deterministic and local, accounts, both qualitatively and quantitatively, for matter-wave duality, quantum criticality, quantum entanglement and the formation of Bose-Einstein condensates.

We cannot conclude without underscoring the simplicity and beauty of the proposed model, which would have probably impressed Isaac newton, Albert Einstein, Paul Dirac, and other fathers of modern physics, who emphasized the importance of the mathematical simplicity and beauty in

theorizing about the physics of the world, which they believed to be harmonious and simple. The Golden Ratio symmetry revealed at the critical point of transition in kinetic energy, in the quantum and cosmic sectors alike deserves special given the key role played by the Golden Ratio and the related Fibonacci numbers as ordering and symmetry numbers in esthetics and arts [131-133], biology [134], brain sciences [135-136], the social sciences [137-139], and more. We believe that the emergence of these numbers in many systems in the physical and social world might be associated with some optimal self-organization processes common to all dynamical system in equilibrium.

The model's scale independency with respect to the velocity of the information carrier is no less intriguing, since it holds the promise of successful applications of the model to classical systems of bodies moving with relatively low velocities and communicating information with relatively low velocities, including acoustic, thermodynamic and seismic systems. No less important it suggest that quantum phenomena might have their replicas in the same rules governing quantum phenomena, as phase transition and entanglement apply to cosmic structures and to classical systems. ,

It seems to us that the proposed epistemic model is the closest model to what is usually termed "a theory of everything", except the fact that it has no axioms, rendering the term theory inappropriate.

We are puzzled as to how mere observations and measures of observables concerning initially moving bodies, regardless of their dimensions and velocities was strikingly successful in predicting the documented dynamics of very small and very large objects. It is as if mere observations, unbiased by theoretical axioms, are most powerful tools for understanding how the physical world behaves. What seems to us astounding, is the fact that the simple recipe of comparing the observations, as they were registered by two observers who are in constant relative motion with respect to each other, seems to reveal not only gross phenomena, like the amount of dark energy or the radius of a black hole, but also Nano-scale phenomena, like quantum phase change, quantum entanglement, and even the Bose-Einstein condensate phenomena, resulting from many-particle

quantum thermodynamic interactions. To what extent the Nature's book could be read from looking at its cover is still to be seen in the future.

References

[1] O'Connor J. J., Roberston E. F. Christian Andreas Doppler- MacTutor History of Mathematics archive. University of St. Andrews (1998).

[2] Maulik D. Doppler Ultrasound in Obstetrics and Gynecology. Springer-Verlag (2005).

[3] Einstein, A., Podolsky, B., & Rosen, N. Can quantum-mechanical description of physical reality be considered complete? *Physical Review*, 47, 777-780 (1935).

[4] Olsen S. *The Golden Section*. New York, Walker & Co. (2006).

[5] Livio M. *The Golden Ratio: The Story of Phi, the World's Most Astonishing Number*. New York, Broadway Books (2002).

[6] Michelson A.A., & Morley E. On the relative motion of the Earth and the luminiferous ether. *American Journal of Science*, 34, 333-345 (1887).

[7] Frisch, D., & Smith, J.H. Measurement of the Relativistic Time Dilation Using µ-Mesons. *American Journal of Physics*, 31, 342-355 (1963).

[8] J. C. Hafele and R. E. Keating. Around-the-World Atomic Clocks: Predicted Relativistic Time Gains. *Science*, Vol. 177, No. 4044, pp. 166-168 (1972).

[9] Wang, R, Zheng, Y., Yao, A., & Langley, D. Modified Sagnac experiment for measuring travel-time difference between counter-propagating light beams in a uniformly moving fiber. *Physics Letters* A, 312 7–10 (2003).

[10] Wang, R., Zheng, Yi, & Yao, A. Generalized Sagnac effect. *Phys. Rev. Lett*., 93 (14), 143901 (2004).

[11] Adam T., et al. Measurement of the neutrino velocity with the OPERA detector in the CNGS beam (OPERA Collaboration). *Journal of High Energy Physics*, 10, 093 (2012).

[12] Adam, T., et al. Measurement of the neutrino velocity with the OPERA detector in the CNGS beam using the 2012 dedicated data. *Journal of High Energy Physics*, 1126-6708 (2013).

[13] Antonello, M., et al. Measurement of the neutrino velocity with the ICARUS detector at the CNGS beam. *Physics Letters B*, 713 (1), 17–22 (2012).

[14] Agafonova, N.Yu., et al. Measurement of the velocity of neutrinos from the CNGS beam with the Large Volume Detector. *Physical Review Letters*, 109, 070801 (2012).

[15] Alvarez Sanchez, P., et al. Measurement of CNGS muon neutrino speed with Borexino. *Physics Letters B*. 716, 401–405 (2012).

[16] Adamson P. et al. Measurement of neutrino velocity with the MINOS detectors and NuMI neutrino beam. (MINOS Collaboration). *Physical Review* D, 76 (7), (2007).

[17] Miller, D.C. Ether-drift experiments at t Wilson. *Proceedings of the National Academy of Sciences USA*, 11(6), 306–314 (1925).

[18] Tomaschek, R. Über das verhalten des lichtes außerirdischer lichtquellen. *Annalen der Physik*, 378, 105–126 (1924).

[19] Illingworth, K. K. A repetition of the Michelson-Morley experiment using Kennedy's refinement. *Physical Review*, 30(5), 692-696 (1927).

[20] Piccard, A. & Stahel, E. L'expérience de Michelson, réalisée en ballonlibre. *Comptes Rendus*, 183(7), 420–421 (1926).

[21] Michelson, A. A., Pease, F. G. & Pearson, F. Results of repetition of the Michelson-Morley experiment. *Journal of the Optical Society of America*, 18(3), 181 (1929).

[22] Joos, G. Die Jenaer Wiederholung des Michelsonversuchs. *Annalen der Physik*, 399 (4), 385–407 (1930).

[23] Newman, A. The special theory disproved by flawed experiment measuring muon decay times. *The General Science Journal*. http://www.gsjournal.net/old/weuro/newman2.pdf (2010).

[24] Sagnac, M. G. C. R. Acad. Sci. 157, 708–710 (1913).

[25] Anderson, R., Bilger, H. R., Stedman, G. E. "Sagnac" effect: A century of Earth-rotated interferometers. *American Journal of Physics*, 62, 11, 975-985 (1994).

[26] Ashby, N. *Relativity in Rotating Frames*, Springer (2004).

[27] Post, E. J. *Rev. Modern Phys.* 39, 475–493 (1967).

[28] Malykin, G. B. Earlier studies of the Sagnac effect. *Phys.-Usp.*, 40 317 (1997).

[29] Ashby, N. Relativity and the Global Positioning System. *Physics Today*, 41-47 (2002).

[30] Chow, W.W. et al. The ring laser gyro. *Reviews of Modern Physics*, 57 (1), 61-104 (1985).

[31] Vali, V., & Shorthill, R. *Appl. Opt.* 16, 290 (1977).

[32] Leeb, W., Schiffner, G., & Scheiterer, E. *Appl. Opt.* 18, 1293 (1979).

[33] Lefevre, H. *The Fiber-Optic Gyroscope*. Artech House: Boston (1993).

[34] Burns, W. K. *Fiber Rotation Sensing*, Academic Press, Boston (1994).

[35] Logunov, A. A., & Chugreev, Y. V. Special theory of relativity and the Sagnac effect, *Sov. Phys. Usp.*, 31 861 (1988).

[36] Ashtekar, A., & Magnon, A. The Sagnac effect in general relativity. *J. Math. Phys.*, 16, 341 (1975).

[37] Adam T., et al. Measurement of the neutrino velocity with the OPERA detector in the CNGS beam. (OPERA Collaboration), arXiv:1109.4897 (2011).

[38] Ekert, A., *Phys. Rev. Lett* 67, 661 (1991).

[39] Naik, D. S. et al. Quantum Cryptography: Eavesdropping on the Ekert Protocol. *Phys. Rev. Lett*, 84, 4733 (2000).

[40] Bennett, C. H., & Wiesner, S. J. *Phys. Rev. Lett*, 69, 2881 (1992).

[41] Mattle, K., Weinfurter, H., Kwiat, P. G., & Zeilinger, A. Dense Coding in Experimental Quantum Communication. *Phys. Rev. Lett*, 76, 4656 (1996).

[42] Boschi, D., et al. *Phys. Rev. Lett*, 80, 1121 (1998).

[43] Bouwmeester, D., et al. *Nature*, 390, 575 (1997).

[44] Barrett, M. D., et al. *Nature*, 429, 737 (2004).

[45] Marcikic, I., H. et al. *Phys. Rev. Lett*, 93, 180502 (2004).

[46] Bell, J. S. On the Einstein Podolsky Rosen paradox, *Physics*, 1 (3), 195 – 200 (1964).

[47] Bell, J.S. Speakable and unspeakable in quantum mechanics, 2nd Editionn. *Cambridge University Press*, Cambridge (2004).

[48] Horodecki, R. Horodecki, P. Horodecki, M., & Horodecki K. Quantum entanglement. *Rev. Mod. Phys*. 81, 865 (2009).

[49] Einstein, A., Podolsky, B., & Rosen, N. Can quantum-mechanical description of physical reality be considered complete? *Physical Review*, 47, 777-780 (1935).

[50] Norsen, T. Local Causality and Completeness: Bell vs. Jarrett. Found Phys., 39, 273-294 (2009).

[51] Aspect, A., Dalibard, J. & Roger, G. Experimental test of Bell's Inequalities using time- varying analyzers. *Phys. Rev. Lett*. 49, 1804-1807 (1982).

[52] Weihs, G., Jennewein, T., Simon, C., Weinfurter, H. & Zeilinger, A. Violation of Bell's Inequality under strict Einstein locality conditions. *Phys. Rev. Lett*. 81, 5039-5043 (1998).

[53] Matsukevich, D. N., Maunz, P., Moehring, D. L., Olmschenk, S. & Monroe, C. Bell Inequality Violation with Two Remote Atomic Qubits. *Phys. Rev. Lett*. 100, 150404 (2008).

[54] Giustina, M. et al. Bell violation using entangled photons without the fair-sampling assumption. *Nature*, 497, 227-230 (2013).

[55] Hensen et al. Loophole-free Bell inequality violation using electron spins separated by 1.3 kilometers, *Nature*, 562, 682-686 526 (2015).

[56] Hardy, L. Quantum mechanics, local realistic theories, and Lorentz-invariant realistic theories. *Phys. Rev. Lett*. 68, 2981(1992).

[57] Berndl, K., Dürr, D., Goldstein, S., and Zanghì, N. Nonlocality, Lorentz Invariance, and Bohmian Quantum Theory. *Phys. Rev*. A 53, 2062–2073 (1996).

[58] de Broglie, L. Waves and quanta. *Nature*, 112, 540 (1923).

[59] de Broglie, L. The reinterpretation of wave mechanics, Foundations of Physics, 1, 5-15 (1970).

[60] Hardy L. Nonlocality of a single photon revisited. *Phys. Rev. Lett*., 73, 2279–2283 (1994).

[61] Coldea R., Tennant D. A., Wheeler E. M., Wawrzynska E., Prabhakaran D., Telling M., Habicht K., Smeibidl P., Kiefer K. Quantum criticality in an Ising chain: Experimental evidence for emergent E8 symmetry. *Science*, 327 (5962), 177–180 (2010).

[62] Schoreder, M. *Fractals, Chaos, Power Laws*. W. Freedman and Company (1991).

[63] Wall, H. S. *Analytic Theory of Continued Fractions*. New York: Chelsea, (1948).

[64] Hausdorff, F. Dimension und äusseres Mass", Mathematische Annalen. 79, 157-179 (1918).

[65] Titchmarsh, E. C., & Heath-Brown, D. R. *The theory of the Riemann zeta-function*. Oxford University Press (1986).

[66] Edwards, H. M. *Riemann's zeta function*, Courier Corporation (2001).

[67] Ketterle, W., Durfee, D. S., & Stamper-Kurn, D. M. Making, probing and understanding Bose-Einstein condensates. arXiv:cond-mat/9904034 v2 5 Apr (1999).

[68] Cornell, E. A., & Wieman, C. E. Nobel Lecture: Bose-Einstein condensation in a dilute gas, the first 70 years and some recent experiments. *Reviews of Modern Physics*, 74, 875-893 (2002).

[69] Vedra, V. Quantifying entanglement in macroscopic systems. *Nature*, 453, 1004-1007 (2008).

[70] Bengtsson, I., Zyczkowski, K. *Geometry of Quantum States: An Introduction to Quantum Entanglement.* Cambridge University Press (2006).

[71] Suleiman, R. The Dark Side Revealed: A Complete Relativity Theory Predicts the Content of the universe. *Progress in Physics, 4,* 34-40 (2013).

[72] Kazanas, D. *Astrophys. J*. 241, L59 (1980).

[73] Guth, A. H. *Phys. Rev*. D 23, 347 (1981).

[74] Sato, K. *Phys. Lett*. B 99, 66 (1981).

[75] K. Greisen, *Phys. Rev. Lett*. 16, 748 (1966).

[76] G. T. Zatsepin and V. A. Kuz'min, *J. Exp. Theor. Phys. Lett*. 4, 78 (1966).

[77] Abbasi, R. U. et al. First Observation of the Greisen-Zatsepin-Kuzmin Suppression. *Phys. Rev. Lett*., 100 (10), 101101 (2008).

[78] Bergman, D.R., et al. Can experiments studying ultrahigh energy cosmic rays measure the evolution of the sources? astro-ph/,DanaInfo=arXiv.org+0603797v1 (2006).

[79] Thomson, G. The TA and TALE experiments. *Journal of Physics: Conference Series* 47, 248 - 254 (2006).

[80] Gilli, R., Cimatti, A., Daddi, E., et al. *ApJ*, 592, 721 (2003).

[81] M. A. Lawrence et al., *J. Phys*. G 17, 733 (1991).

[82] M. I. Pravdin et al., in Proc. 26th ICRC, 3, 292 (1999).

[83] M. Takeda et al., *Astropart. Phys*. 19, 447 (2003).

[84] K. Shinozaki, An AGASA reanalysis in which the number of events above 1020 eV is reduced from 11 to 6, Proc. *Quarks* (2006).

[85] Albrecht, A. et al. Report of the Dark Energy Task Force. *Astro. Ph*. 0609591 (2006)

[86] Linder E.V. Probing gravitation, dark energy, and acceleration. *Phys. Rev*. D, 2004, 70 (2), 023511, [11 pages] (2004).

[87] Sandvik H. B., Barrow J. D., Magueijo J.A Simple Cosmology with a Varying Fine Structure Constant. *Phys. Rev. Lett*., 88, 031302 [4 pages] (2002).

[89] Easson D. A. Framptona P. H., Smoota G. F. Entropic accelerating universe. *Physics Letters* B, 696, 3 (31), 273–277 (2011).

[89] Wittman, D. M., et al. Detection of weak gravitational lensing distortions of distant galaxies by cosmic dark matter at large scales. *Nature*, 405, 143-148 (2000).

[90] Samushia, L., & Ratra, B. Constraints on dark energy models from radial baryon acoustic scale measurements. *The Astrophysical Journal*, 701, 373–1380 (2009).

[91] Farooq, M. O. Observational constraints on dark energy cosmological model parameters. (Preprint) arXiv:1309.3710 (2013).

[92] Kunz, M, & Bassett, B. A. A tale of two distances. (Preprint) arXiv: astro-ph/0406013 (2004).

[93] Furlanetto, S. R. The global 21-centimeter background from high redshifts. *Mon. Not. R. Astron. Soc*. 371, 867–878 (2006).

[94] Oguri, M., et al. The Sloan digital sky survey quasar lines search. III Constrains on dark energy from the third data released quasar lens catalog. *The Astronomical Journal*, 135, 512–519 (2008).

[95] Viel, M, Haehnelt, M.G., & Springel, V. Inferring the dark matter power spectrum from the Lyman α forest in high-resolution QSO absorption spectra. *Mon. Not. R. Astron*. Soc. 354, 684 – 694 (2004).

[96] Michell, J. On the Means of discovering the Distance, Magnitude, etc. of the Fixed Stars, in consequence of the Diminution of the velocity of their Light, in case such a Diminution should be found to take place in any of them, and such Data should be procured from Observations, as would be farther necessary for that Purpose. *Philosophical Transactions*, 74: 35-57 (1784).

[97] Laplace, P. *Exposition du System du Monde*, Paris: Cercle-Social (1796).

[98] K. Schwarzschild. Über das Gravitationsfeld eines Massenpunktes nach der Einsteinschen Theorie, *Sitzungsberichte der Deutschen Akademie der Wissenschaften zu Berlin, Klasse fur Mathematik, Physik, und Technik*, pp 189 (1916).

[99] Hawking, S. W. Black Hole Explosions? *Nature*, 248: 30-31 (1974).

[100] Bekenstein, J. D. Black Holes and Entropy. *Physical Review D* 7: 2333-2346 (1973).

[101] Bowyer, S. et al. Cosmic X-ray Sources, *Science*, 147 (3656): 394–398 (1965).

[102] Xiong, D. R., & Zhang, X. The connections between bulk Lorentz factor, black hole mass and accretion in Fermi FSRQs. *Astrophysics and Space Science*, DIO: 10.1007/s 10509 (2014).

[103] Ferrarese, L., & Ford, H. Supermassive Black Holes in Galactic Nuclei: Past, Present and Future Research. *Space Science Reviews*, 116 (3-4): 523-624 (2005).

[104] John Kormendy, J., & Richstone, D. Inward bound − The search for supermassive black holes in galactic neuclei. *Annu. Rev. Astron. Astrophys.*, 33:581-624 (1995).

[105] Doeleman, S., et al. Jet-launching structure resolved near the supermassive black Hole in M87. *Science*, 338: 355 − 358 (2012).

[106] Ferrarese, L., & Merritt, D. A fundamental relation between supermassive black holes and their host galaxies. *The Astrophysical Journal*, 539:L9–L12 (2000).

[107] Chokshi, A., & Turner, E. L. Remnants of the quasars. *Mon. Not. R. Astr. Soc*. 259: 421- 424 (1992).

[108] Di Matteo, T., Springel, V., & Hernquist, L. Energy input from quasars regulates the growth and activity of black holes and their host galaxies. *Nature*, 433, 604-607 (2005).

[109] Bardeen, J. *Proceedings of GR5*, Tiflis, U.S.S.R. (1968).

[110] Borde, A. *Phys. Rev*. D., 50, 3392 (1994).

[111] Borde, A., *Phys. Rev*., D55, 7615 (1997).

[112] Ay´on–Beato, E., Asymptotic Behavior of Scalar Fields Coupled to Gravity, Graduate Dissertation, Faculty of Physics, Havana Univ. (1993).

[113] Barrab`es, C., Frolov, V.P., *Phys. Rev*., D53, 3215 (1996).

[114] Mars, M., Mart´ın–Prats, M.M., Senovilla, J.M.M., Class. *Quant. Grav*., 13, L51 (1996).

[115] Cabo, A., Ay´on–Beato, E., *Int. J. Mod. Phys*., A14, 2013 (1999).

[116] Ayon-Beato, E., Garcia, A. Regular black hole in general relativity coupled to nonlinear electrodynamics. *Phys. Rev. Lett*., 80, 5056 (1998).

[117] Tseytlin, A.A., *Phys. Lett*., B363, 223 (1995).

[118] Callan, Jr. C. G., & Maldacena, J. M. D-Brane Approach to Black Hole Quantum Mechanics. *Nuclear Physics* B, 489, 65–94 (1997).

[119] Ashtekar, E., & Bojowald, M. Quantum geometry and the Schwarzschild singularity. *Class. Quantum Grav.* 23, 391. doi:10.1088/0264-9381/23/2/008 (2006).

[120] Ashtekar A., Pawlowski, T., & Singh, P. Quantum nature of the big bang: An analytical and numerical study. *Phys. Rev. Lett*., 96, 141301 (2006).

[121] Bojowald, M. Absence of singularity in loop quantum cosmology. *Phys. Rev. Lett.* 86, 5227 - 5230 (2001).

[122] Ashtekar A, Bojowald M and Lewandowski J. Mathematical structure of loop quantum cosmology. *Adv. Theor. Math. Phys*. 7, 233–268 (2003).

[123] Hawking, S. W. Particle creation by black holes", *Communications in Mathematical Physics*, 43, 199-220 (1975).

[124] K. Hurley, K. et al. Interplanetary network localization of GRB 991208 and the discovery of its afterglow. *The Astrophysical Journal Letters*, 534, doi:10.1086/312645 (2000).

[125] Steinhardt, C. L., et al. SDSS 0956+5128: A broad-line quasar with extreme velocity offsets. *ApJ* 759 24, doi:10.1088/0004-637X/759/1/24 (2012).

[126] Calderone, at al. B2 0954+25A: a typical Fermi blazar or a γ -ray loud Narrow Line Seyfert 1? Mon. Not. R. *Astron. Soc*. 424, 3081–3093 (2012).

[127] Xiong, D.R., & Zhang, X. The connections between bulk Lorentz factor, black hole mass and accretion in Fermi FSRQs. *Astrophysics and Space Science*, DOI 10.1007/s10509-014- 1967-y, (2014).

[128] Matsuoka, M. X-ray observations of high-z radio loud/quiet quasars. *A & Space Res*. 23, 1151-l 154 (1999).

[129] Elíasdóttir, Á., et al. Dust extinction in high-z galaxies with gamma-ray burst afterglow spectroscopy: the 2175 Å feature at z= 2.45. *The Astrophysical Journal*, 697:1725–1740 (2009).

[130] Hook, I. M. (Ed.), The science case for the European Extremely Large Telescope: The next step in mankind's quest for the Universe. *The Messenger*, 121, 2-10 (2005).

[131] Green, C. D. All that glitters: a review of psychological research on the aesthetics of the golden section. *Perception*, 24 (8), 937 – 968 (1995).

[132] Pittard, N., Ewing, M., & Jevons, C. Aesthetic theory and logo design: examining consumer response to proportion across cultures. *International Marketing Review*, 24(4), 457- 473 (2007).

[133] Hammel, G. T., & Vaughan, K. C. *Math and Music: Harmonious Connections*. Dale Seymour Publications (1995).

[134] Klar, A. J. S. Fibonacci's flowers. *Nature*, 417, 595 (2002).

[135] Weiss, H., & Weiss, V. The golden mean as clock cycle of brain waves. *Chaos, Solitons, & Fractals*, 18(4), 643- 652 (2003).

[136] Roopun, A. K., Kramer, M. A., Carracedo, L. M., Kaiser, M., Davies, C. H., Traub, R. D., Kopell, N. J., & Whittington, M. A. Temporal interactions between cortical rhythms. *Frontiers in Neuroscience*, 2 (2), 145-154 (2008).

[137] Lefebvre, V. A. The golden section and an algebraic model of ethical cognition. *Journal of Mathematical Psychology*, 29 (3), 289 -310 (1985).

[138] Suleiman, R. On religious pro-sociality, fairness, and beauty. *Proceedings of the 2nd International Conference on Science, Technology and Art Relations*. (2015).

[139] Nikolic, S.T., Cosic, L., Pecujlija, M., & Miletic, A. The effect of the Golden Ratio on consumer behavior. *African Journal of Business Management*, 5, 8347-8360 (2011).

Supplementary Information

1. Derivation of Epistemic Relativity Transformations

A. Derivation of the Time Transformation

We consider a simple preparation in which the time duration of an event, as measured by an observer A who is stationary with respect to the point of occurrence of the event in space, is transmitted by an information carrier which has a constant and known velocity v_c, to an observer B who is moving with constant velocity v with respect to observer A. We make no assumptions about nature of the information carrier, which can be either a wave of some form or a small or big body of mass. Aside of the preparation describes above and the measurements taken by each observer, throughout the entire analysis to follow, no further assumptions are made. This also means that we do not undertake any logical steps or mathematical calculations unless measurements of the variables involved in such steps or calculations are experimentally measurable.

We ask: what is the event duration time to be concluded by each observer, based on his or her own measurements of time? And what could be said about the relationship between the two concluded durations?

In a more formal presentation, we consider two observers in two reference frames F and F'. For the sake of simplicity, but without loss of generality, assume that the observers in F and F' synchronizes their clocks, just when they start distancing from each other with constant velocity v, such that $t_1 = t_1' = 0$, and that at time zero in the two frames, origin points of were F and F' were coincided (i.e., $x_1 = x_1' = 0$).

Suppose that at time zero in the two frames, an event started occurring in F' at the point of origin, lasting for exactly $\Delta t'$ seconds according to the clock stationed in F',

and that promptly with the termination of the event, a signal is sent by the observer in F' to the observer in F.

After $\Delta t'$ seconds, the point at which the event took place stays stationary with respect F' (i.e., $x_2' = x_1' = 0$), while relative to frame F this point would have departed by x_2 equaling:

$$x_2 = v\,\Delta t' \hspace{3cm} \text{……. (1a)}$$

The validity of eq. 1a could be checked and verified by more than one operational, i.e., experimentally feasible methods: For example, if the two observers meet any time after the event has terminated, then the observer in F will be able to read the time of the event as registered by the clock stationed in F' and learned what the duration of the event in F', for which the event was stationary. Another operational way by which the observer in F can infer about the actual time of travel until the event terminated and the signal was sent is by mimicking the even in F by having an identical event with the same duration (in its inertial frame), start promptly with the even in F'. It is important to note that the above two operational suggestions presume the rule stating that the laws of nature are the same in the two frames. In the first example, the above restriction leaves no possibility for the observer in F to suspect that the reading of the clock stationed F' in e time duration of the event in reading of the clock at F' (in the first example), or to suspect that a time registered by a clock at his/her own frame F will differ by the time that will be registered for an identical event, by an identical clock placed in F'.

If the information carrier sent from the observer in F' to the observer in F travel with constant velocity V_F relative to F, then it will be received by the observer in F after a delay of:

$$t_d = \frac{x_2}{V_F} = \frac{v\,\Delta t'}{V_F} = \frac{v}{V_F}\,\Delta t' \qquad\qquad \text{........ (2a)}$$

Since F' is distancing from F with velocity v, we can write:

$$V_F = V_0 - v \qquad\qquad \text{...... (3a)}$$

Where V_0 denotes the information carrier's velocity with respect to the event's inertial frame F'. Substituting the value of V_F from eq. 3a in eq. 2a, we obtain:

$$t_d = \frac{v\,\Delta t'}{V_0 - v} = \frac{1}{\frac{V_0}{v} - 1}\,\Delta t' \qquad\qquad \text{...... (4a)}$$

Due to the information time delay, the event's time duration Δt that will be registered by the observer in F is given by:

$$\Delta t = \Delta t' + t_d = \Delta t' + \frac{1}{\frac{V_0}{v} - 1}\,\Delta t' = \left(1 + \frac{1}{\frac{V_0}{v} - 1}\right)\Delta t' = \left(\frac{\frac{V_0}{v}}{\frac{V_0}{v} - 1}\right)$$

$$= \left(\frac{1}{1 - \frac{v}{V_0}}\right)\Delta t' \qquad\qquad \text{...(5a)}$$

Or:

$$\frac{\Delta t}{\Delta t'} = \frac{1}{1 - \frac{v}{V_0}} \qquad\qquad \text{... (6a)}$$

For $v \ll V_0$ eq. 6 reduces to the classical Newtonian equation $\Delta t = \Delta t'$, while for $v \rightarrow V_0$, $\Delta t \rightarrow \infty$ for all positive $\Delta t'$.

For a communication medium to be fit for transmitting information between frames in relative motion, a justifiable condition is to require that the velocity of the carrier is larger than the velocity of the relative motion, i. e., $v < V_0$.

Quite interestingly, eq. (6a), derived for the time travel of moving bodies with constant velocity is quite similar to the Doppler's Formula derived for the frequency modulation of waves emitted from traveling bodies. Importantly, in both cases **the direction of motion matters**. In the Doppler Effect a wave emitted from a distancing body will be red-shifted (longer wavelength), whereas a wave emitted from an approaching body with be blues-shifted (shorter wavelength). In both cases the degree of red or blue shift will be positively correlated with the body's velocity.

The same applies to the time duration of an event occurring at a stationary point of a moving frame. If the frame is distancing from the observer, time will be dilated, whereas if the frame is approaching the observer will contract.

It is especially important to note further that the above derived transformation applies to *all* carriers of information, including the commonly employed *acoustic* and *optical* communication media. For the case in which information is carried by light or by electromagnetic waves with equal velocity, equation (6a) becomes:

$$\frac{\Delta t}{\Delta t'} = \frac{1}{1 - \frac{v}{c}} \qquad \qquad \text{..... (7a)}$$

Since an objection might be raised for the cases of information translation by means of light or other waves with equal velocity, such objection could be avoided by restricting the theoretical model derived above to wave propagation in mediums that are not a vacuum, which in fact the case in almost all physical situations of interest.

B. Derivation of the Distance Transformation

To derive the distance transformation, consider the two frames of reference F and F' shown in Figure 1b. Assume the two frames are moving away from each other at a constant velocity v. Assume further that at time t_1 in F (and t_1' in F'), a body starts moving in the $+x$ direction from point x_1 (x_1' in F') to point x_2 (x_2' in F'), and that its arrival is signaled by a light pulse that emits exactly when the body arrives at its destination. Denote the internal framework of the emitted light by F_0. Without loss of generality, assume $t_1 = t_1' = 0$, $x_1 = x_1' = 0$. Also denote $t_2 = t$, $t_2' = t'$, $x_2 = x$, and $x_2' = x'$.
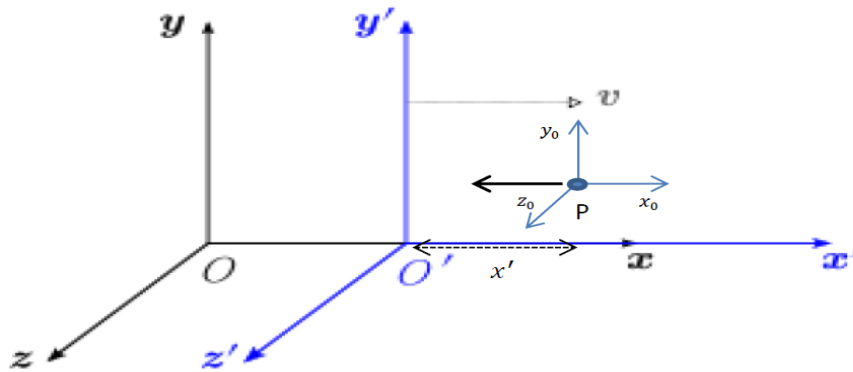

Figure 1b: Two observers in two reference frames, moving with velocity v with respect to each other.

From eq. 7a, the time duration in F that takes the light signal to reach an observer in F' equals:

$$\Delta t_p = \left(1 - \left(-\frac{v}{c}\right)\right) \Delta t' \qquad \qquad \text{..... (1b)}$$

Where $\Delta t'$ is the corresponding time duration in F', and c is the velocity of light in frame F. Because F' is moving away from F with velocity v, the time that takes the light signal to reach and observer in F is equal to:

$$\Delta t = \Delta t_p + \frac{v\Delta t}{c} = \Delta t_p + \frac{v}{c}\,\Delta t \qquad\qquad \text{...... (2b)}$$

Substituting Δt_p from eq. 1b in eq. 2b yields:

$$\Delta t = (1 + \frac{v}{c})\,\Delta t' + \frac{v}{c}\,\Delta t, \qquad\qquad \text{..... (3b)}$$

or:

$$\frac{\Delta t}{\Delta t'} = \frac{(1+\frac{v}{c})}{(1-\frac{v}{c})}\ . \qquad\qquad \text{...... (4b)}$$

But $\Delta x = c.\Delta t$ and $\Delta x' = c.\Delta t'$. Thus, we can write:

$$\frac{\Delta x}{\Delta x\prime} = \frac{(1+\frac{v}{c})}{(1-\frac{v}{c})} \qquad\qquad \text{....... (5b)}$$

C. Derivation of the Mass and Energy Transformations

Consider the two frames of reference F and F' shown in Figure 3a. Suppose that the two frames are moving relative to each other at a constant velocity v. Consider a uniform cylindrical body of mass m_0 and length of l_0 placed in F' along its travel direction. Suppose that at time t_1 the body leaves point x_1 (x_1' in F') and moves with constant velocity v in the $+x$ direction, until it reaches point x_2 (x_2' in F') in time t_1 (x_2' in F'). The body's density in the internal frame F' is given by: $\rho' = \dfrac{m_0}{A\, l_0}$, where A is the area of the body's cross section, perpendicular to the direction of movement.

In F the density is given by: $\rho = \dfrac{m_0}{Al}$, where l is the object's length in F. Using the distance transformation (eq. 8a) l could be written as:

$$l = \frac{1+\beta}{1-\beta}\, l_0 \qquad\qquad \text{...... (1c)}$$

Thus, we can write: $\rho = \dfrac{m_0}{Al} = \dfrac{m_0}{A\, l_0\, (\frac{1+\beta}{1-\beta})} = \rho_0 \left(\dfrac{1-\beta}{1+\beta}\right)$ .... (2c)

Or,

$$\frac{\rho}{\rho_0} = \frac{1+\beta}{1-\beta} \qquad\qquad \text{.... (3c)}$$

The kinetic energy of a *unit of volume* is: given by:

$$e_k = \frac{1}{2}\rho\, v^2 = \frac{1}{2}\rho_0\, c^2\, \frac{(1-\beta)}{(1+\beta)}\beta^2 = e_0\, \frac{(1-\beta)}{(1+\beta)}\beta^2 \qquad \text{.... (4c)}$$

Where $e_0 = \dfrac{1}{2}\rho_0\, c^2$.

For $\beta \to 0$ (or $v \ll c$) eq. 3c reduces $\rho = \rho_0$, and the kinetic energy expression (eq. 4c) reduces to Newton's expression $e = \frac{1}{2}\rho_0 v^2$. Figures 1c depict the relativistic energy as functions of β.
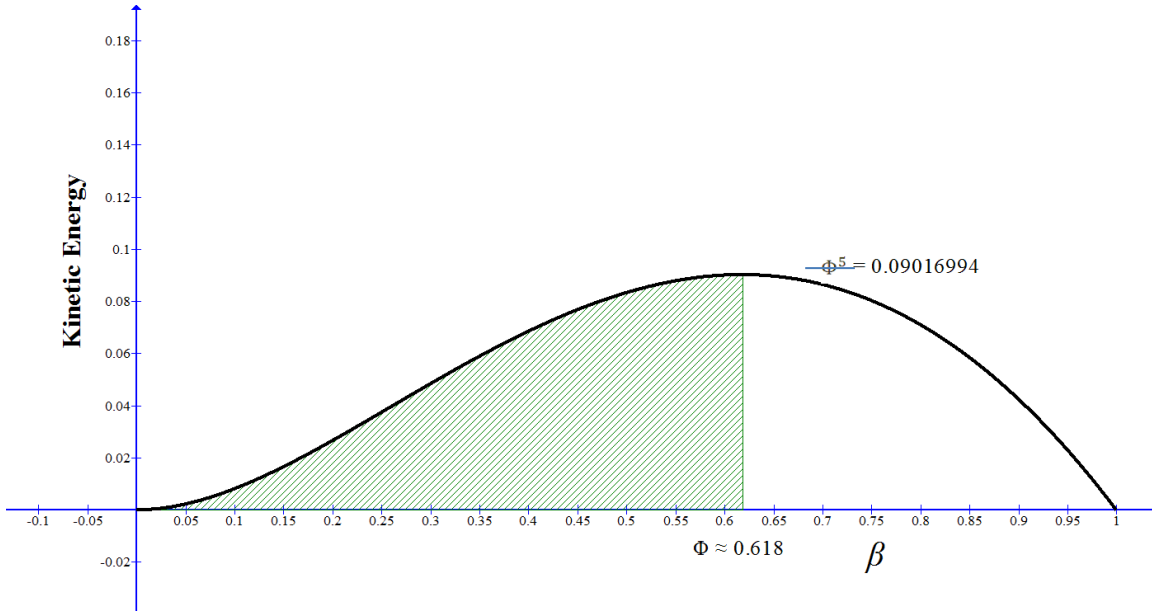

Figure 1c. Kinetic energy as a function of velocity

As shown by the figure the relativistic kinetic energy of *distancing* bodies relative to an observer in *F* is predicted to *decrease* with β, approaching zero as $\beta \to 1$, while the density in F for *approaching* bodies is predicted to increase with β, up to extremely high values as $\beta \to -1$. Strikingly, for distancing bodies the kinetic energy displays a non-monotonic behavior. It increases with β up to a maximum at velocity $\beta = \beta_{cr}$, and then decreases to zero at $\beta = 1$. Calculating β_{cr} is obtained by deriving eq. 4c with respect to β and equating the result to zero, yielding:

$$\frac{d}{d\beta}\left(\beta^2 \frac{(1-\beta)}{(1+\beta)}\right) = 2\beta \frac{(1-\beta)}{(1+\beta)} + \beta^2 \frac{[(1+\beta)(-1)-(1-\beta)(1)]}{(1+\beta)^2}$$

$$= 2\beta \frac{(1-\beta^2-\beta)}{(1+\beta)^2} = 0 \qquad\qquad .....(5c)$$

65

For $\beta \neq 0$ and we get:

$$\beta^2 + \beta - 1 = 0 \qquad \text{… (6c)}$$

Which solves for:

$$\beta_{cr} = \frac{\sqrt{5}-1}{2} = \Phi \approx 0.618 \qquad \text{… (7c)}$$

Where Φ is the Golden Ratio. Substituting β_{cr} in the energy expression (eq. 4c) yields:

$$(e_k)_{max} = e_0 \; \Phi^2 \frac{1-\Phi}{1+\Phi} \qquad \text{…. (8c)}$$

From eq. 6c we can write: $\Phi^2 + \Phi - 1 = 0$, which implies $1 - \Phi = \Phi^2$ and $1 + \Phi = \frac{1}{\Phi}$.

Substitution in eq. 8c gives:

$$(e_k)_{max} = \Phi^5 e_0 \approx 0.09016994 \; e_0 \qquad \text{…. (9c)}$$

2. Derivation of the term $\frac{v-c}{c}$ for a typical neutrino velocity experiments

For a typical neutrino-velocity experiment, consider a neutrino that travels a distance d from a source (e.g., at CERN) and arrives at a detector (e.g., at Gran Sasso). According to Epistemic Relativity Epistemic Relativity, such an experiment includes *three* frames: the neutrino frame F, the source frame F', and the detector frame F''. F is departing from F' with velocity v and approaching F'' with velocity $-v$. F' and F'' are at rest relative to each other. To derive the term $\frac{v-c}{c}$ for a typical neutrino velocity experiments we use eq. 4 to write:

$$\Delta t_S = \frac{\Delta t}{1-\frac{v}{c}}, \qquad \text{…… (1d)}$$

And

$$\Delta t_D = \frac{\Delta t}{1-\frac{-v}{c}} = \frac{\Delta t}{1+\frac{v}{c}} \qquad \qquad \text{...... (2d)}$$

Where v is the neutrino velocity, c is the velocity of light. Δt, Δt_S, and Δt_D are the times, as measured in frames F (neutrino rest-frame), F' (source), and F'' (detector), respectively.

The neutrino time of flight tof_v is equal to difference between the times as measured in the detector and the source, or:

$$tof_v = \frac{d}{v} = \frac{\Delta t}{1+\frac{v}{c}} - \frac{\Delta t}{1-\frac{v}{c}} = -\frac{2\frac{v}{c}}{1-(\frac{v}{c})^2}. \qquad \qquad \text{.... (3d)}$$

Where d is the travel distance. For an *early* neutrino arrival time, δt, with respect to the velocity of light, we can write:

$$\frac{d}{c} - \delta t = tof_v = -\frac{2\frac{v}{c}}{1-(\frac{v}{c})^2}\frac{d}{v}. \qquad \qquad \text{..... (4d)}$$

Solving for $\frac{v}{c}$ yields

$$\frac{v}{c} = \left(\frac{2}{1-\frac{c\,\delta t}{d}} - 1\right)^{\frac{1}{2}}, \qquad \qquad \text{.... (5d)}$$

Or:

$$\frac{v-c}{c} = \sqrt[2]{\frac{2}{1-\frac{c\,\delta t}{d}} - 1} - 1 \qquad \qquad \text{....(6d)}$$